Supporting Information

Title: Unlocking the Significance of High H_2O Resistance for Nickel Vanadate Phases to Improve Kinetic Parameters or Consequences of Catalytic NO_X Reduction and Poison Pyrolysis

Authors: Seokhyun Lee,[ab] Heon Phil Ha,[a] Jung-Hyun Lee,[b] and Jongsik Kim[c]*

* jkim40@khu.ac.kr; Tel.: (+82) 31-201-2444.

Affiliations:

[a] Extreme Materials Research Center, Korea Institute of Science and Technology, Seoul, 02792, South Korea.

[b] Department of Chemical & Biological Engineering, Korea University, Seoul, 02841, South Korea.

[c] Department of Chemical Engineering, Kyung Hee University, Yongin, 17104, South Korea.

Table of Contents

Experimental section

Catalysts

The catalysts were synthesized using wet impregnation technique, whose procedures depicted in our previous studies[1-4] were slightly modified. In the case of TiO_2-supported $Ni_1V_2O_6$ (Ni_1), $Ni_2V_2O_7$ (Ni_2), or $Ni_3V_2O_8$ (Ni_3) catalyst, 'A' g of TiO_2 (DT51, CristalACTiV^{TM}) was mixed with 170 mL of de-ionized H_2O and stirred at 25 °C for half an hour before being further mixed with 2.36 mmol of NH_4VO_3 (≥ 99.0 %, Junsei) and 2.36 mmol of $(COOH)_2{\cdot}2H_2O$ (oxalic acid, 99.5-100 %, Junsei), both of which were dissolved in 70 mL of de-ionized H_2O (A of 5.81 g for Ni_1; 5.74 g for Ni_2; 5.67 g for Ni_3). The resulting mixture was then stirred at 25 °C for half an hour, mixed with 'B' mmol of $Ni(NO_3)_2{\cdot}3H_2O$ (≥ 97.0 %, Junsei) dissolved in 70 mL of de-ionized H_2O, stirred at 25 °C for 18 hours, subjected to rotary evaporation for the removal of de-ionized H_2O, dried at 110 °C for 18 hours, and calcined at 500 °C for 5 hours with a ramping rate of 5 °C min^{-1} (B of 1.18 mmol for Ni_1; 2.36 mmol for Ni_2; 3.54 mmol for Ni_3). Meanwhile, 12.3 mmol of $Sb(CH_3COO)_3$ (≥ 97.0 %, Alfa Aesar) was dissolved in 500 mL of CH_3COOH (acetic acid, 99.5-100.5 %, J. T. Baker), stirred at 25 °C for half an hour, mixed with 48.5 g of TiO_2, stirred at 25 °C for 18 hours, subjected to rotary evaporation for the removal of acetic acid, dried at 110 °C for 18 hours, and calcined at 500 °C for 5 hours with a ramping rate of 5 °C min^{-1} for the production of antimony oxide supported on TiO_2 (Sb/TiO_2).[1-4] Sb-promoted Ni_1 catalyst (Ni_1-Sb) was then synthesized according to the protocols identical to those utilized to synthesize Ni_1 except for the use of Sb/TiO_2 as a support. WO_3-promoted V_2O_5 supported on TiO_2 (V_2O_5-WO_3) was synthesized according to the protocols we reported elsewhere[1, 2, 4] and served to simulate a commercial catalyst. The catalyst finally underwent surface modification with SO_Z^{2-}/HSO_Z^- (Z= 3-4) functionalities, for which the catalyst was exposed to 500 ppm SO_2/3 vol. % O_2/N_2 at 500 °C for an hour with a total flow rate of 500 mL min^{-1} and a ramping rate of 10 °C min^{-1}.[1-6] This led to the generation of SO_Z^{2-}/HSO_Z^--modified Ni_1 (Ni_1-S), Ni_2 (Ni_2-S), Ni_3 (Ni_3-S), Ni_1-Sb (Ni_1-Sb-S), or V_2O_5-WO_3 (V_2O_5-WO_3-S).

Characterizations

X-ray diffraction (XRD) patterns of the catalysts were acquired on a D8 Advance diffractometer (Bruker) with the analytic conditions of 20-80° for 2θ range, 0.02° per step for step size, 2 seconds per step for scan speed in addition to the use of Cu K_α radiation with the wavenumber of 0.154 nm. X-ray fluorescence (XRF) analysis of the catalysts were performed on a ZSX Primus II spectrometer (Rigaku). High-resolution transmission electron microscopy (HRTEM) images and selected area electron diffraction (SAED) patterns of the catalysts were acquired on a Titan 80-300™ (FEI) with the acceleration voltage of 300 keV after the catalyst surfaces were purged under vacuum (~10^{-7} mmHg). Energy-dispersive X-ray spectroscopy (EDX) mapping images of the catalysts were acquired using an Ultim max 170 (Oxford) at 15 kV after the catalyst surfaces were purged under vacuum (~10^{-6} mmHg). X-ray photoelectron spectroscopy (XPS) spectra of the catalysts were acquired with the resolution of 0.05 eV on a PHI 5000 VersaProbe after the catalyst surfaces were purged under vacuum (~10^{-4} mmHg). XPS spectra of the catalysts were curve-fitted using Gaussian function, with which adventitious carbon band situated at binding energy centered at ~284.6 eV was used as a reference to correct binding energies of XPS spectra in the Ni 2p, V 2p, S 2p, and O 1s regimes. (See Table S2.) Temperature-resolved Raman spectra of the catalysts were acquired under a N_2 at 25 °C or 220 °C with the resolution of 0.3 cm^{-1} on an inVia Raman Microscope (Renishaw) coupled with X 50 objective lens and a 532 nm excitation laser after the catalyst surfaces were purged with a N_2 at 300 °C for half an hour with a total flow rate of 300 mL min^{-1} and a ramping rate of 10 °C min^{-1}.[3] Raman spectra of the catalysts were curve-fitted using Gaussian function.[3] N_2 isotherms of the catalysts were acquired on a NOVA 2200e (Quantachrome Instruments) at -196 °C after the catalyst surfaces were purged under vacuum (2 X 10^{-3} mmHg). Brunauer-Emmett-Teller (BET) and Barrett-Joyner-Halenda (BJH) theories were utilized to evaluate N_2-accessible BET surface areas ($S_{BET, N2}$; $m_{N2}^2\ g_{CAT}^{-1}$) and pore volumes ($V_{PORE, N2}$; $cm_{N2}^3\ g_{CAT}^{-1}$) of the catalysts, respectively, for which the catalyst surfaces were purged at 150 °C under vacuum (2 X 10^{-3} mmHg). The quantities of N_2 adsorbed on the catalyst surfaces at partial pressure (P/P_0) domain of 0.05-0.3 were considered to assess $S_{BET, N2}$ values of the catalysts.[7] H_2O isotherms of the catalysts were acquired on a BELSORP-MAX (MicrotracBEL Corp.) at 10-40 °C. H_2O-accessible BET surface areas in a per-gram basis ($S_{BET, H2O}$; $m_{H2O}^2\ g_{CAT}^{-1}$) or in a per-H_2O-accessible site basis (S_{H2O}; $m_{H2O}^2\ mol_{H2O}^{-1}$) for the

catalysts were evaluated with the contemplation of the numbers of H_2O adsorbed on the catalyst surfaces (N_{H2O}; $mol_{H2O}\ g_{CAT}^{-1}$) at P/P_0 domain of 0.05-0.3 and 10 °C.[8-13] S_{H2O} values of the catalysts correspond to their $S_{BET,\ H2O}$ values divided by N_{H2O} values at P/P_0 of ~1.0 and 10 °C.[10-15] Moreover, H_2O isotherms of the catalysts were fitted using Toth equation (Eqn. S1), in which $N_{H2O,\ 0}$ is referred to as the maximum amount of H_2O adsorbed in a per-gram of the catalyst ($mol_{H2O}\ g_{CAT}^{-1}$), whereas C, D, and P indicate constant indigenous to the catalyst (bar^{-1}), constant associated with heterogeneity of the catalyst surface (unit-less), and pressure (bar), respectively,[10-15] as detailed in Table S7. Isosteric heats of H_2O adsorption on the catalyst surfaces at near-zero H_2O coverage (E_{H2O}) were evaluated using Clausius-Clapeyron equation (Eqn. S2), where P_A/P_B and R are referred to as pressures (bar) at temperatures of T_A/T_B (K) and ideal gas constant (8.3145 J mol^{-1} K^{-1}), respectively.[10, 11, 14-16]

$$N_{H2O} = N_{H2O,0} \times \frac{C \times P}{(1 + (C \times P)^D)^{(\frac{1}{D})}} \quad (S1)$$

$$ln\left(\frac{P_A}{P_B}\right) = \frac{E_{H2O}}{R} \times \left(\frac{T_A - T_B}{T_A \times T_B}\right) \quad (S2)$$

Background-subtracted *in situ* diffuse reflectance infrared Fourier transform (DRIFT) spectra of the catalysts were acquired with the resolution of 4 cm^{-1} on an FT/IR/4200 (Jasco) equipped with KBr optics and a mercury-cadmium-telluride (MCT) detector. The catalyst was placed in a reaction cell (Harrick Scientific), purged with 3 vol. % O_2/N_2 at 300 °C for half an hour, and exposed to 250 °C (or 500 °C) under a N_2 for the collection of background signal at 250 °C (or 500 °C) with a ramping rate of 10 °C min^{-1}. Background-subtracted *in situ* DRIFT spectrum of the catalyst was then collected under 1,000 ppm NH_3/N_2 (at 250 °C), 1,000 ppm NO/3 vol. % O_2/N_2 (at 250 °C) or under 1,000 ppm SO_2/3 vol. % O_2/N_2 (at 500 °C) with a total flow rate of 200 mL min^{-1}. CO-pulsed chemisorption experiments of the catalysts were conducted on an Autochem II (Micromeritics) at 50 °C, for which 10 °C min^{-1} served as a ramping rate. The catalyst surfaces were purged with 10 vol. % O_2/He at 300 °C for an hour, cooled to 50 °C under a He, and subjected to periodic CO injection at 50 °C till thermal conductivity detector (TCD) signals of CO were invariant.[1-6] O_2-pulsed chemisorption experiments of the catalysts were also carried out on an Autochem II (Micromeritics) at 250 °C, for which 10 °C min^{-1} served as a ramping rate.[3] The catalyst surfaces were purged with 10 vol. % O_2/He at 300 °C for an hour, cooled to 50 °C under a He, reduced under 10 vol. % H_2/He at 300 °C for an hour, cooled to 250 °C under a He, and subjected to periodic O_2 injection at 250 °C till TCD signals of O_2 were unaltered.[3] O_2-, NH_3-, or SO_2-temperature-programmed desorption (TPD) profiles of the catalysts were acquired on an Autochem II (Micromeritics), an Autochem II coupled with an on-line mass spectrometer (HPR20, Hiden Analytical), or an Autochem II connected to a quartz reactor coupled with an on-line SO_2 analyzer (ZKJ-2 (Fuji Electric Co.). In the case of O_2-TPD experiments with a ramping rate of 10 °C min^{-1} except for that utilized during the final stage, the catalyst surface was purged with 10 vol. % O_2/He at 300 °C for an hour, cooled to 50 °C under a He, and reduced under 10 vol. % H_2/He at 300 °C for an hour, cooled to 250 °C under a He, exposed to 10 vol. % O_2/He at 250 °C for an hour to ensure the saturation of O_2-accessible surface sites with O_2 prior to the exposure of the surface to a He at 250 °C for an hour to eliminate O_2 physisorbed on the surface.[3] The surface was finally heated to 600 °C under a He with a ramping rate (β) of 10 °C min^{-1}, 20 °C min^{-1}, or 30 °C min^{-1} for acquiring a profile of TCD signal of O_2 released versus temperature for the catalyst at a β value set.[3-6, 17] O_2-TPD profiles at dissimilar β values were then curve-fitted using Gaussian function to reveal two sub-bands (denoted as I and II in Table S5) with desorption temperatures (T_{MAX}), at which maximum intensities of TCD signals were observed.[3-6, 17] Binding energy between the surface and O_2 adsorbed ($E_{OL/OM}$) was assessed with the use of TPD theory (Eqn. S3), where $\theta_{OL/OM,\ MAX}$ and ν_n/n are referred to as surface O_2 coverage at T_{MAX} and lumped constants indigenous to the surface, respectively.[3-6, 17] Plot of ln (β/T_{MAX}^2) versus ($1/T_{MAX}$) for sub-band I or II provided a slope identical to ($-E_{OL/OM}/R$) with the postulation concerning the independence of $E_{OL/OM}$ on $\theta_{OL/OM,\ MAX}$ (Table S5).[3-6, 17]

$$\ln\left(\frac{\beta}{T_{MAX}^2}\right) = -\left(\frac{E_{OL/OM}}{R}\right)\left(\frac{1}{T_{MAX}}\right) - 2.303 \times \log\left(\frac{E_{OL/OM}}{\nu_n Rn\, \theta_{OL/OM,MAX}^{n-1}}\right) \quad (S3)$$

In the case of NH_3-TPD experiments with NH_3 chemisorption at 150 °C and a ramping rate of 10 °C min^{-1} except for that utilized during the final stage, the catalyst surface was purged with 10 vol. % O_2/He at 300 °C for an

hour, cooled to 150 °C under a He, exposed to 5 vol. % NH_3/He at 150 °C for an hour to ensure the saturation of NH_3-accessible surface sites with NH_3 prior to the exposure of the surface to a He at 150 °C for an hour to eliminate NH_3 physisorbed on the surface.[3-6, 17] The surface was finally heated to 700 °C under a He with a ramping rate (β) of 10 °C min^{-1}, 20 °C min^{-1}, or 30 °C min^{-1} for acquiring a profile of NH_3 (m/z~ 17) signal released versus temperature for the catalyst at a β value set.[3-6, 17] NH_3-TPD profiles at dissimilar β values were then curve-fitted using Gaussian function to reveal three sub-bands (denoted as I, II, and III in Table S3) with desorption temperatures (T_{MAX}), at which maximum intensities of NH_3 (m/z~ 17) signals were observed.[3-6, 17] Binding energy between the surface and NH_3 adsorbed (E_{NH3}) was assessed with the use of TPD theory (Eqn. S4), where $\theta_{NH3,\ MAX}$ and ν_n/n are referred to as surface NH_3 coverage at T_{MAX} and lumped constants indigenous to the surface, respectively.[3-6, 17] Plot of ln (β/T_{MAX}^2) versus ($1/T_{MAX}$) for sub-band I, II, or III provided a slope identical to ($-E_{NH3}/R$) with the postulation concerning the independence of E_{NH3} on $\theta_{NH3,\ MAX}$ (Table S3).[3-6, 17]

$$\ln\left(\frac{\beta}{T_{MAX}^2}\right) = -\left(\frac{E_{NH3}}{R}\right)\left(\frac{1}{T_{MAX}}\right) - 2.303 \times \log\left(\frac{E_{NH3}}{\nu_n R n \theta_{NH3,MAX}^{n-1}}\right) \quad (S4)$$

In the case of NH_3-TPD experiments with NH_3 chemisorption at 50 °C and a ramping rate of 10 °C min^{-1}, the catalyst surface was purged with 10 vol. % O_2/He at 300 °C for an hour, cooled to 50 °C under a He, exposed to 5 vol. % NH_3/He at 50 °C for an hour to ensure the saturation of NH_3-accessible surface sites with NH_3 prior to the exposure of the surface to a He at 50 °C for an hour to eliminate NH_3 physisorbed on the surface. The surface was finally heated to 700 °C under a He for acquiring a profile of NH_3 (m/z~ 17) signal released versus temperature for the catalyst. In the case of SO_2-TPD experiment with SO_2 chemisorption at 220 °C and a ramping rate of 10 °C min^{-1}, the catalyst surface was purged with 10 vol. % O_2/He at 300 °C for an hour, cooled to 220 °C under a He, exposed to 5,000 ppm SO_2/N_2 at 220 °C for an hour to ensure the saturation of SO_2-accessible surface sites with SO_2 prior to the exposure of the surface to a He at 220 °C for an hour to eliminate SO_2 physisorbed on the surface. The surface was finally heated to 900 °C under a He for acquiring a profile of SO_2 concentration released versus temperature for the catalyst. H_2-temperature-programmed reduction (TPR) profiles of the catalysts were acquired on an Autochem II (Micromeritics). While a ramping rate was set to 10 °C min^{-1}, the catalyst surface was purged with 10 vol. % O_2/He at 300 °C for an hour, cooled to 50 °C under a He, and reduced to 900 °C under 10 vol. % H_2/He for acquiring a profile of TCD signal versus temperature for the catalyst. A thermo-gravimetric analyzer (TGA2, Mettler-Toledo, denoted as TGA) equipped with an on-line mass spectrometer (HPR20, Hiden Analytical, denoted as MASS) were utilized to conduct TGA-MASS experiments of the catalysts poisoned with AS/ABS.[2, 4] The poisoned catalyst was situated in an Al_2O_3 pan, purged with an Ar at 100 °C for an hour, and heated to 600 °C under an Ar with a flow rate of 50 mL min^{-1} and a ramping rate of 2 °C min^{-1} for acquiring a series of profiles concerning weight loss/NH_3 signal (m/z~ 17)/H_2O signal (m/z~ 18)/SO_2 signal (m/z~ 64) released versus temperature for the catalyst.[2, 4]

Reactions

Initially, the catalyst sieved with sizes of 200-300 μm or 300-425 μm was placed inside a quartz reactor with an inner diameter of 0.4 cm, wherein the amount of the catalyst loaded was altered to regulate the control volume and/or space velocity (*e.g.*, 0.31 g/0.62 g of catalyst → 0.5 mL/1 mL of control volume → 60,000 hr^{-1}/30,000 hr^{-1} of space velocity). The quartz reactor was then loaded in a tube furnace, purged with 3 vol. % O_2/N_2 at 400 °C for an hour, and subjected to control SCR or SO_2 oxidation runs under a feed gas stream including N_2, NO_X, NH_3, O_2, H_2O, or SO_2 with variable compositions alongside with the use of a total flow rate of 500 mL min^{-1} and a reaction temperature of ≤ 400 °C. Effluents emitted from the control volume were monitored using ZKJ-2 (Fuji Electric Co.) for NO/SO_2, Ultramat 6 (Siemens Co.) for N_2O, and detector tubes (GASTEC Co.) for NO_2/NH_3. NO_X conversion (X_{NOX}) and N_2 selectivity (S_{N2}) of the catalyst were evaluated using Eqn. S5 and S6, wherein $C_{YYY,\ IN}$ and $C_{YYY,\ OUT}$ are referred to as concentrations of species YYY at the inlet (IN) and outlet (OUT), respectively.

$$X_{NOX}\ (\%) = \frac{C_{NO,IN} - C_{NO,OUT} - C_{NO2,OUT} - 2 \times C_{N2O,OUT}}{C_{NO,IN}} \times 100 \quad (S5)$$

$$S_{N2}\ (\%) = \frac{C_{NO,IN} + C_{NH3,IN} - C_{NO,OUT} - C_{NH3,OUT} - C_{NO2,OUT} - 2 \times C_{N2O,OUT}}{C_{NO,IN} + C_{NH3,IN} - C_{NO,OUT} - C_{NH3,OUT}} \times 100 \ (S6)$$

NO_X consumption rate ($-r_{NOX}$) in a per-NH_3-accessible site for the catalyst was evaluated using Eqn. S7, in which the quantity of NH_3-accessible sites in a per-gram of the catalyst (N_{NH3}) can be evaluated via its NH_3-TPD experiment with NH_3 chemisorption at 150 °C (Table S4).[2-4, 6, 17] $-r_{NOX}$ generically corresponds to Eqn. S8, in which k_{APP} and C_{NOX}, C_{NH3}, C_{O2} indicate the apparent reaction rate constant, NO_X concentration, NH_3 concentration, and O_2 concentration, respectively, whereas α/β/γ denote the reaction orders with respect to $NO_X/NH_3/O_2$.[3, 4, 6] Arrhenius plot of ln ($-r_{NOX}$) versus $1/T_{REACTION}$ for the catalyst (Eqn. S9) provides a slope ($-E_{BARRIER}/R$) and y-intercept (ln ($k_{APP,\,0}C_{NOX}^{\alpha}C_{NH3}^{\beta}C_{O2}^{\gamma}$)), by which the energy barrier ($E_{BARRIER}$) and lumped pre-factor ($k_{APP,\,0}C_{NOX}^{\alpha}C_{NH3}^{\beta}C_{O2}^{\gamma}$; $k'_{APP,\,0}$) required to proceed with SCR are evaluated at reaction temperatures ($T_{REACTION}$) considered, respectively.[3, 4, 6]

$$-r_{NOX}\ (min^{-1}) = \frac{moles\ of NO_X\ reduced\ per\ gram\ of\ the\ catalyst\ per\ unit\ time\ (\Delta mol_{NOX}\ g_{CAT}^{-1}\ min^{-1})}{N_{NH3}\ (mol_{NH3}\ g_{CAT}^{-1})}\ (S7)$$

$$-r_{NOX}\ (min^{-1}) = k_{APP}\, C_{NOX}^{\alpha} C_{NH3}^{\beta} C_{O2}^{\gamma}\ (S8)$$

$$ln\ (-r_{NOX}) = (-\frac{E_{BARRIER}}{R}) \times \left(\frac{1}{T_{REACTION}}\right) + ln\ \underbrace{(k_{APP,0} C_{NOX}^{\alpha} C_{NH3}^{\beta} C_{O2}^{\gamma})}_{lumped\ pre-factor}\ (S9)$$

AS/ABS degradation rate ($-r_{AS/ABS}$) in a per-NH_3-accessible site for the catalyst was assessed using Eqn. S10, for which weight lost above NH_3 onset temperature presumably originates from ABS degradation, whereas N_{NH3} was contemplated because NH_3-accessible sites were identified to function as major active species in catalyzing AS/ABS degradation.[4] In addition, TGA-MASS data above SO_2 onset temperature was also considered for the evaluation of $-r_{AS/ABS}$ for the catalyst, given the rate-determining stage of catalytic AS/ABS degradation pathway we reported elsewhere (*i.e.*, H_2-assisted dissociative desorption of $H^+\bullet\bullet^-O\text{-}SO_2\text{-}O^-\bullet\bullet H^+$ from $B^-\text{-}H^+\bullet\bullet^-O\text{-}SO_2\text{-}O^-\bullet\bullet H^+$, where B^- denote conjugate base of Brönsted acidic bond ($B^-\text{-}H^+$) in Fig. 1D).[4] In this regard, weight lost at 260 °C, 270 °C, 280 °C, or 290 °C with temperature deviation of ± ~0.5 °C (time interval (Δt) of ≤ ~0.5 minutes) was considered to assess $-r_{AS/ABS}$ of the catalyst (Table S8).[4] $-r_{AS/ABS}$ can be expressed using a generic n^{th}-order reaction rate law, where $k_{AS/ABS,\,APP}$ and $C_{AS/ABS}$ denote apparent reaction rate constant and AS/ABS concentration, respectively.[4] Arrhenius plot of ln ($-r_{AS/ABS}$) versus $1/T_{REACTION}$ for the catalysts (Eqn. S11) provides a slope ($-E_{BARRIER}/R$) and y-intercept (ln ($k_{AS/ABS,\,APP,\,0}C^{n}_{AS/ABS}$)), in which $E_{BARRIER}$ and $k_{AS/ABS,\,APP,\,0}C^{n}_{AS/ABS}$ ($k'_{AS/ABS,\,APP,\,0}$) indicate the energy barrier and lumped pre-factor needed to proceed with AS/ABS degradation at $T_{REACTION}$ values considered, respectively.[4]

$$-r_{AS/ABS}\ (min^{-1}) = \frac{moles\ of\ ABS\ decomposed\ per\ gram\ of\ the\ catalyst\ (\Delta mol_{ABS}\ g_{CAT}^{-1})}{N_{NH3}\ of\ catalyst\ (mol_{NH3}\ g_{CAT}^{-1}) \times time\ interval\ (\Delta t)\ used\ to\ measure\ \Delta mol_{ABS}\ g_{CAT}^{-1}\ (min)}\ (S10)$$

$$ln\ (-r_{AS/ABS}) = (-\frac{E_{BARRIER}}{R}) \times \left(\frac{1}{T_{REACTION}}\right) + ln\ \underbrace{(k_{AS/ABS,APP,0} C_{AS/ABS}^{n})}_{lumped\ pre-factor}\ (S11)$$

Table S1. Properties of the catalysts.

	Ni_1	Ni_2	Ni_3	Ni_1-Sb	Ni_1-S	Ni_2-S	Ni_3-S	Ni_1-Sb-S
V [a] (wt. %)	2.2 (± 0.1)	2.1 (± 0.1)	2.2 (± 0.1)	2.2 (± 0.1)	2.2 (± 0.1)	2.1 (± 0.1)	2.3 (± 0.1)	2.3 (± 0.1)
Ni [a] (wt. %)	1.3 (± 0.1)	2.6 (± 0.1)	3.8 (± 0.1)	1.2 (± 0.1)	1.2 (± 0.1)	2.3 (± 0.1)	3.6 (± 0.1)	1.2 (± 0.1)
S [a] (wt. %)	-	-	-	-	0.7 (± 0.1)	0.7 (± 0.1)	1.1 (± 0.1)	0.6 (± 0.1)
Ni/V (bulk) [a, b]	0.5 (± 0.1)	0.9 (± 0.1)	1.5 (± 0.1)	0.5 (± 0.1)	0.5 (± 0.1)	1.0 (± 0.1)	1.5 (± 0.1)	0.5 (± 0.1)
Ni/V (surface) [b, c]	0.5 (± 0.1)	1.0 (± 0.1)	1.5 (± 0.1)	0.5 (± 0.1)	0.5 (± 0.1)	0.9 (± 0.1)	1.5 (± 0.1)	0.5 (± 0.1)
Ni/V (surface) [b, d]	0.5 (± 0.1)	1.0 (± 0.1)	1.4 (± 0.1)	0.6 (± 0.1)	0.5 (± 0.1)	1.1 (± 0.1)	1.4 (± 0.1)	0.5 (± 0.1)
S/metal (bulk) [a, b, e]	-	-	-	-	0.3 (± 0.1)	0.3 (± 0.1)	0.4 (± 0.1)	0.3 (± 0.1)
S/metal (surface) [b, c, e]	-	-	-	-	0.4 (± 0.1)	0.4 (± 0.1)	0.5 (± 0.1)	0.4 (± 0.1)
S/metal (surface) [b, d, e]	-	-	-	-	0.5 (± 0.1)	0.4 (± 0.1)	0.4 (± 0.1)	0.5 (± 0.1)
$S_{BET, N2}$ [f, g] (m_{N2}^2 g_{CAT}^{-1})	82.8 (± 6.4)	79.9 (± 4.2)	79.6 (± 3.5)	82.0 (± 5.3)	64.4 (± 3.4)	61.2 (± 5.4)	69.2 (± 1.8)	59.1 (± 3.4)
$V_{PORE, N2}$ [f, h] (cm_{N2}^3 g_{CAT}^{-1})	0.4 (± 0.1)	0.4 (± 0.1)	0.4 (± 0.1)	0.3 (± 0.1)	0.3 (± 0.1)	0.3 (± 0.1)	0.3 (± 0.1)	0.3 (± 0.1)
N_{CO} [i] (μmol_{CO} g_{CAT}^{-1})	1.7 (± 0.1)	11.1 (± 0.4)	14.6 (± 2.3)	2.6 (± 0.1)	1.4 (± 0.1)	5.4 (± 0.2)	8.6 (± 0.1)	0.6 (± 0.1)
N_{O2} [j] (μmol_{O2} g_{CAT}^{-1})	307.4 (± 11.6)	410.6 (± 9.5)	443.3 (± 4.3)	330.3 (± 9.7)	260.3 (± 4.1)	351.3 (± 8.1)	409.8 (± 12.3)	280.0 (± 5.3)

[a] via XRF. [b] molar ratio. [c] via XPS spectroscopy (Fig. S2). [d] via EDX mapping. [e] metal of Ni+V for Ni_1-S, Ni_2-S, Ni_3-S; Ni+V+Sb for Ni_1-Sb-S. [f] via N_2 physisorption at -196 °C (Fig. S1). [g] via BET theory. [h] via BJH theory. [i] via CO-pulsed chemisorption at 50 °C (Fig. S9). [j] via O_2-pulsed chemisorption at 250 °C (Fig. S15).

Table S2. Binding energies and relative abundance of surface phases observed in XPS spectra of the catalysts.

		Ni_1	Ni_2	Ni_3	Ni_1-Sb	Ni_1-S	Ni_2-S	Ni_3-S	Ni_1-Sb-S
				Ni 2p $_{1/2}$ [a, b, c]					
Ni^{2+} (marked with ●)	binding energy (eV)				872.0				
	relative abundance (%)	73.3	62.5	58.8	70.4	76.9	71.0	67.7	80.2
Ni^{3+} (marked with ●)	binding energy (eV)				874.6				
	relative abundance (%)	26.7	37.5	41.2	29.6	23.1	29.0	32.3	19.8
				Ni 2p $_{3/2}$ [a, b, c]					
Ni^{2+} (marked with ○)	binding energy (eV)				854.3				
	relative abundance (%)	73.3	62.5	58.8	70.4	76.9	71.0	67.7	80.2
Ni^{3+} (marked with ○)	binding energy (eV)				856.7				
	relative abundance (%)	26.7	37.5	41.2	29.6	23.1	29.0	32.3	19.8
				V 2p $_{3/2}$ [a, b, d]					
V^{3+} (marked with ○)	binding energy (eV)				515.2-515.3				
	relative abundance (%)	13.9	15.6	5.3	7.6	6.9	3.5	11.7	7.5
V^{4+} (marked with ○)	binding energy (eV)				516.2-516.3				
	relative abundance (%)	20.0	30.2	44.3	25.1	23.6	32.1	27.8	18.3
V^{5+} (marked with ○)	binding energy (eV)				517.0-517.1				
	relative abundance (%)	66.1	54.2	50.4	67.3	69.5	64.4	60.5	74.2
				O 1s [a, b, e]					
O_β (marked with ○)	binding energy (eV)				529.9				
	relative abundance (%)	63.8	61.9	57.5	50.2	64.4	63.4	63.1	61.4
O_α (marked with ○)	binding energy (eV)				530.6				
	relative abundance (%)	35.1	35.6	36.4	41.9	31.9	31.1	28.1	34.8
O'_α (marked with ○)	binding energy (eV)				532.0				
	relative abundance (%)	1.1	2.5	6.1	7.9	3.7	5.5	8.8	3.8
				S 2p $_{1/2}$ [a, b, f]					
SO_3^{2-} (marked with ●)	binding energy (eV)				167.3				
	concentration (%)	-	-	-	-	11.8	10.3	7.4	10.3
HSO_3^- (marked with ●)	binding energy (eV)				168.3				
	concentration (%)	-	-	-	-	25.0	21.8	22.0	18.7
SO_4^{2-} (marked with ●)	binding energy (eV)				169.5				
	concentration (%)	-	-	-	-	33.8	32.0	29.4	37.4
HSO_4^- (marked with ●)	binding energy (eV)				170.4				
	concentration (%)	-	-	-	-	29.4	35.9	41.2	33.6
				S 2p $_{3/2}$ [a, b, f]					
SO_3^{2-} (marked with ○)	binding energy (eV)				166.1				
	concentration (%)	-	-	-	-	11.8	10.3	7.4	10.3

HSO_3^- (marked with ○)	binding energy (eV)					167.1				
	concentration (%)	-	-	-	-		25.0	21.8	22.0	18.7
SO_4^{2-} (marked with ○)	binding energy (eV)					168.3				
	concentration (%)	-	-	-	-		33.8	32.0	29.4	37.4
HSO_4^- (marked with ○)	binding energy (eV)					169.2				
	concentration (%)	-	-	-	-		29.4	35.9	41.2	33.6

[a] fitted via Gaussian function. [b] peak resolution of 0.05 eV. [c] See Fig. S8. [d] See Fig. S7. [e] See Fig. S14. [f] peak separation of ~1.2 eV. (See Fig. 3.)

Table S3. Ramping rates (β), desorption temperatures (T_{MAX}) with maximum NH_3 signal intensities, and slopes of 'ln (β/T_{MAX}^2) versus $1/T_{MAX}$' for the sub-bands obtained via curve-fits of NH_3-TPD profiles for the catalysts.

sub-band [a]	β (°C min^{-1})	T_{MAX} (°C)			
		Ni_1-S	Ni_2-S	Ni_3-S	Ni_1-Sb-S
I (marked with ○)	10	227.0	227.4	227.4	227.2
	20	228.7	229.6	230.1	229.5
	30	230.8	231.6	231.9	231.4
II (marked with ○)	10	273.2	273.2	275.0	273.1
	20	274.7	275.8	277.8	275.4
	30	277.5	278.0	280.0	278.2
III (marked with ○)	10	350.4	337.0	342.4	336.8
	20	353.6	340.5	346.0	340.2
	30	356.0	342.7	348.7	342.6
sub-band		slope [b, c]			
		Ni_1-S	Ni_2-S	Ni_3-S	Ni_1-Sb-S
I (marked with ○○○○)		-3503.5	-3098.0	-2780.9	-2531.1
II (marked with △△△△)		-3520.3	-3171.2	-3017.8	-2570.3
III (marked with ▽▽▽▽)		-3498.4	-3194.2	-2881.2	-2697.3

[a] via Gaussian function. (See Fig. S11.) [b] via TPD theorem. [c] regression factors of ≥ 0.96. (See Fig. 4B.)

Table S4. NO_X consumption rates ($-r_{NOX}$) of the catalysts

temperature (°C)	$-r_{NOX}$ [a, b] (X 10^{-1} min^{-1})			
	Ni_1-S	Ni_2-S	Ni_3-S	Ni_1-Sb-S
220	1.38 (± 0.09)	0.43 (± 0.01)	0.35 (± 0.02)	1.51 (± 0.01)
235	1.98 (± 0.03)	0.63 (± 0.01)	0.53 (± 0.01)	2.13 (± 0.07)
243	2.23 (± 0.06)	0.75 (± 0.04)	0.63 (± 0.02)	2.47 (± 0.04)
250	2.53 (± 0.06)	0.85 (± 0.01)	0.71 (± 0.03)	2.78 (± 0.07)

[a] SCR conditions: 800 ppm NO_X; 800 ppm NH_3; 3 vol. % O_2; 5.4 vol. % H_2O; catalysts with the sizes with 300-425 µm; space velocity of 300,000 hr^{-1}; total flow rate of 500 mL min^{-1}; balanced by a N_2. [b] X_{NOX} values of < 25 %.

Table S5. Ramping rates (β), desorption temperatures (T_{MAX}) with maximum TCD signal intensities, and slopes of 'ln (β/T_{MAX}^2) versus $1/T_{MAX}$' for the sub-bands obtained via curve-fits of O_2-TPD profiles for the catalysts.

sub-band [a]	β (°C min^{-1})	T_{MAX} (°C)			
		Ni_1-S	Ni_2-S	Ni_3-S	Ni_1-Sb-S
I (marked with ○)	10	421.3	421.4	395.0	380.3
	20	425.0	425.0	398.2	384.0
	30	429.0	428.6	401.3	388.4
II (marked with ○)	10	445.6	452.2	458.1	406.0
	20	450.0	456.0	462.0	410.0
	30	454.0	459.8	465.4	414.5
sub-band		slope [b, c]			
		Ni_1-S	Ni_2-S	Ni_3-S	Ni_1-Sb-S
I (marked with ○○○○)		-2923.0	-3224.0	-3539.3	-2317.9
II (marked with △△△△)		-2798.0	-3316.2	-3572.7	-2378.5

[a] via Gaussian function. (See Fig. S16.) [b] via TPD theorem. [c] regression factors of ≥ 0.99. (See Fig. 7B.)

Table S6. N_2 selectivities (S_{N2}) of the catalysts exposed to wet feed gases with the occasional inclusion of SO_2.

	S_{N2} (%)						
	with H_2O only [a]						
$T_{REACTION}$ (°C)	Ni_1-S [b]	Ni_2-S [b]	Ni_3-S [b]	Ni_1-Sb-S [b]	Ni_1-Sb-S-HT [b]	V_2O_5-WO_3-S [b]	V_2O_5-WO_3-S-HT [b]
450	99.8	99.8	96.8	99.4	-	-	-
500	99.4	99.3	96.8	97.6	-	-	-
	with H_2O and SO_2 [a]						
$T_{REACTION}$ (°C)	Ni_1-S [b]	Ni_2-S [b]	Ni_3-S [b]	Ni_1-Sb-S [b]	Ni_1-Sb-S-HT [b]	V_2O_5-WO_3-S [b]	V_2O_5-WO_3-S-HT [b]
450	100.0	-	-	99.5	97.1	98.5	94.9
500	99.7	-	-	98.2	91.1	93.6	83.0

[a] SCR conditions: 800 ppm NO_X; 800 ppm NH_3; SO_2 of 0 ppm for 'with H_2O only (Fig. 7D)' or 500 ppm for 'with H_2O and SO_2' (Fig. 9B); 3 vol. % O_2; 5.4 vol. % H_2O; catalysts with the sizes with 300-425 μm; space velocity of 60,000 hr^{-1}; total flow rate of 500 mL min^{-1}; balanced by a N_2. [b] S_{N2} of 100 % at 150-400 °C.

Table S7. Coefficients used to fit H_2O isotherms of the catalysts via Toth equation.

catalyst	temperature (°C)	coefficient [a]			regression factor (R^2) [b]
		$N_{H2O,\,0}$ ($mmol_{H2O}\ g_{CAT}^{-1}$)	C (bar^{-1})	D (dimensionless)	
Ni_1-S	10 (marked with ○)	8009524.85	0.19×10^{0}	0.51×10^{-1}	0.99
	25 (marked with ○)	44287.97	0.20×10^{-2}	0.96×10^{-1}	0.99
	40 (marked with ○)	3201.05	0.72×10^{-3}	0.18×10^{0}	0.99
Ni_1-Sb-S	10 (marked with ○)	32247.13	0.46×10^{-4}	0.18×10^{0}	0.99
	25 (marked with ○)	6906.09	0.68×10^{-4}	0.26×10^{0}	0.99
	40 (marked with ○)	10.59	0.20×10^{0}	4.55×10^{0}	0.99

[a] via Toth equation. (See Fig. S18.) [b] using Polymath 6.0.

Table S8. TGA-MASS dataset used to assess $-r_{AS/ABS}$ values of the catalysts poisoned with AS/ABS.

catalyst poisoned with AS/ABS [a]	temperature (°C)	ΔT [b] (°C)	Δt (minute)	ΔAS/ABS [c, d, e] (μmol_{ABS})	$-r_{AS/ABS}$ (X 10^{-2} min^{-1})
V_2O_5-WO_3-S	260	0.53	0.27	2.10	3.1
	270	0.48	0.24	2.10	3.5
	280	0.40	0.20	2.10	4.2
	290	0.35	0.17	2.10	4.8
Ni_1-Sb-S	260	0.38	0.19	2.02	5.3
	270	0.16	0.08	1.01	6.0
	280	0.29	0.14	2.02	6.9
	290	0.13	0.07	1.01	7.5

[a] AS/ABS poison conditions: 800 ppm NO_X; 800 ppm NH_3; 500 ppm SO_2; 3 vol. % O_2; 5.4 vol. % H_2O; 180 °C; 30 hours; catalysts with the sizes with 300-425 µm; space velocity of 60,000 hr^{-1}; total flow rate of 500 mL min^{-1}; balanced by a N_2. [b] deviation of ± 0.5 °C from 260 °C, 270 °C, 280 °C, or 290 °C. [c] under an Ar; total flow rate of 50 mL min^{-1}; ramping rate of 2 °C min^{-1}. [d] assuming that the transition of AS to ABS is complete at < 260 °C. (ABS is assumed to be the sole reactant.) [e] See Fig. S19.

Table S9. AS/ABS tolerance of SO_Z^{2-}-functionalized metal vanadates deposited on Sb/TiO_2.

metal vanadate [a, b]	time-on-stream SCR conditions [c]			reference
	temperature (°C)	space velocity (hr^{-1})	time span to show $X_{NOX}/X_{NOX,\ 0}$~0.8	
$Mn_1V_2O_6$	220	30,000	~17 hours	[2]
$Cu_3V_2O_8$	220	30,000	~16 hours	[3]
$Ni_1V_2O_6$	220	30,000	~53 hours	this work

[a] SO_Z^{2-} functionalization conditions: 500 ppm SO_2; 3 vol. % O_2; catalysts with the sizes with 300-425 μm; space velocity of 60,000 hr^{-1}; total flow rate of 500 ml min^{-1}; ramping rate of 10 °C min^{-1}; 500 °C for an hour; balanced by a N_2. [b] supported on Sb/TiO_2 with Sb contents of 3 wt. %. [c] reaction condition: 800 ppm NO_X; 800 ppm NH_3; 500 ppm SO_2; 3 vol. % O_2; 5.4 vol. % H_2O (for $Mn_1V_2O_6$) or 6 vol. % H_2O (for $Cu_3V_2O_8$); catalysts with the sizes with 300-425 μm; total flow rate of 500 ml min^{-1}, balanced by a N_2.

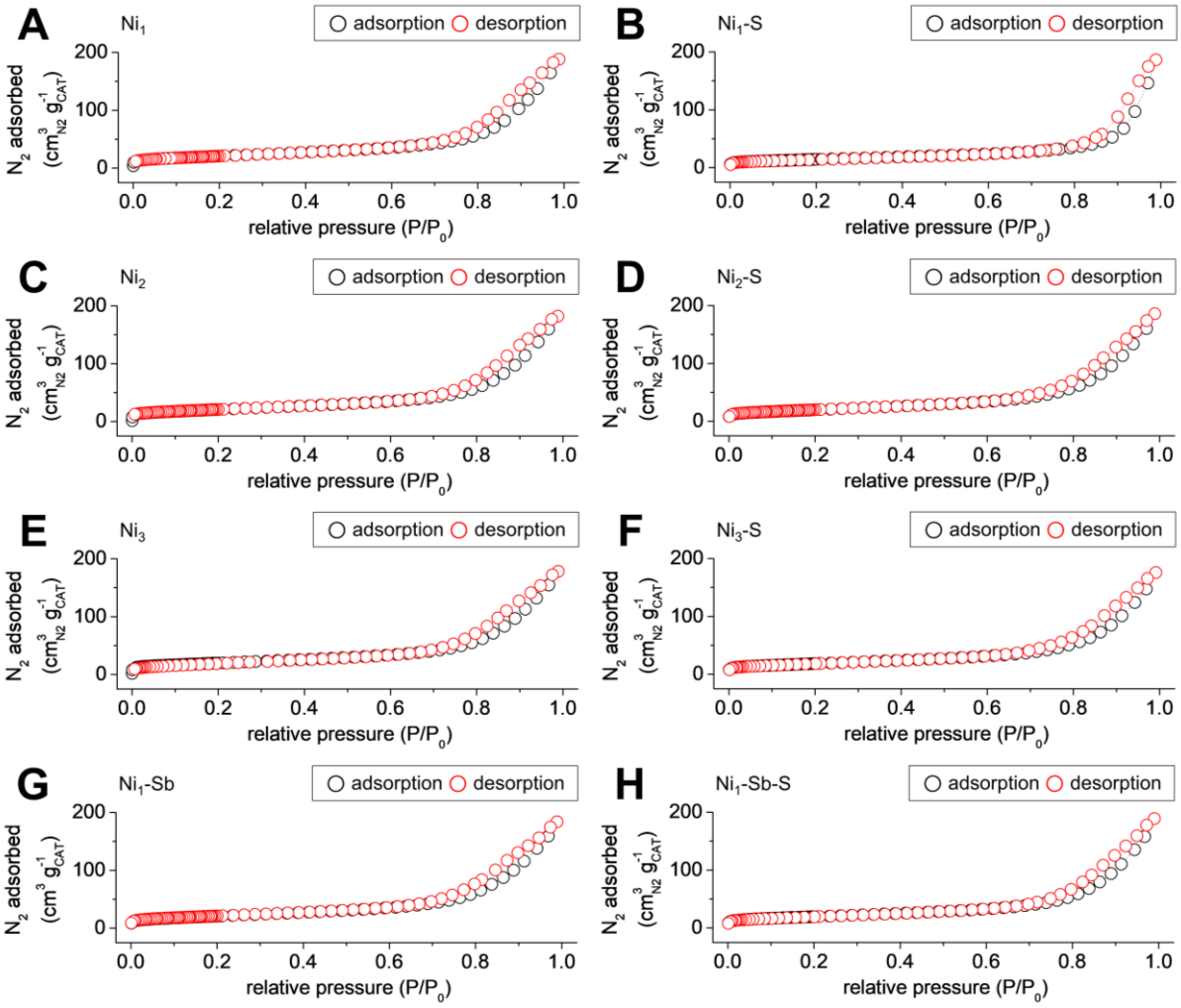

Fig. S1. N_2 isotherms of the catalysts (Ni_1 for A; Ni_2 for C; Ni_3 for E; Ni_1-Sb for G) and those functionalized with SO_Z^{2-}/HSO_Z^- (Ni_1-S for B; Ni_2-S for D; Ni_3-S for F; Ni_1-Sb-S for H).

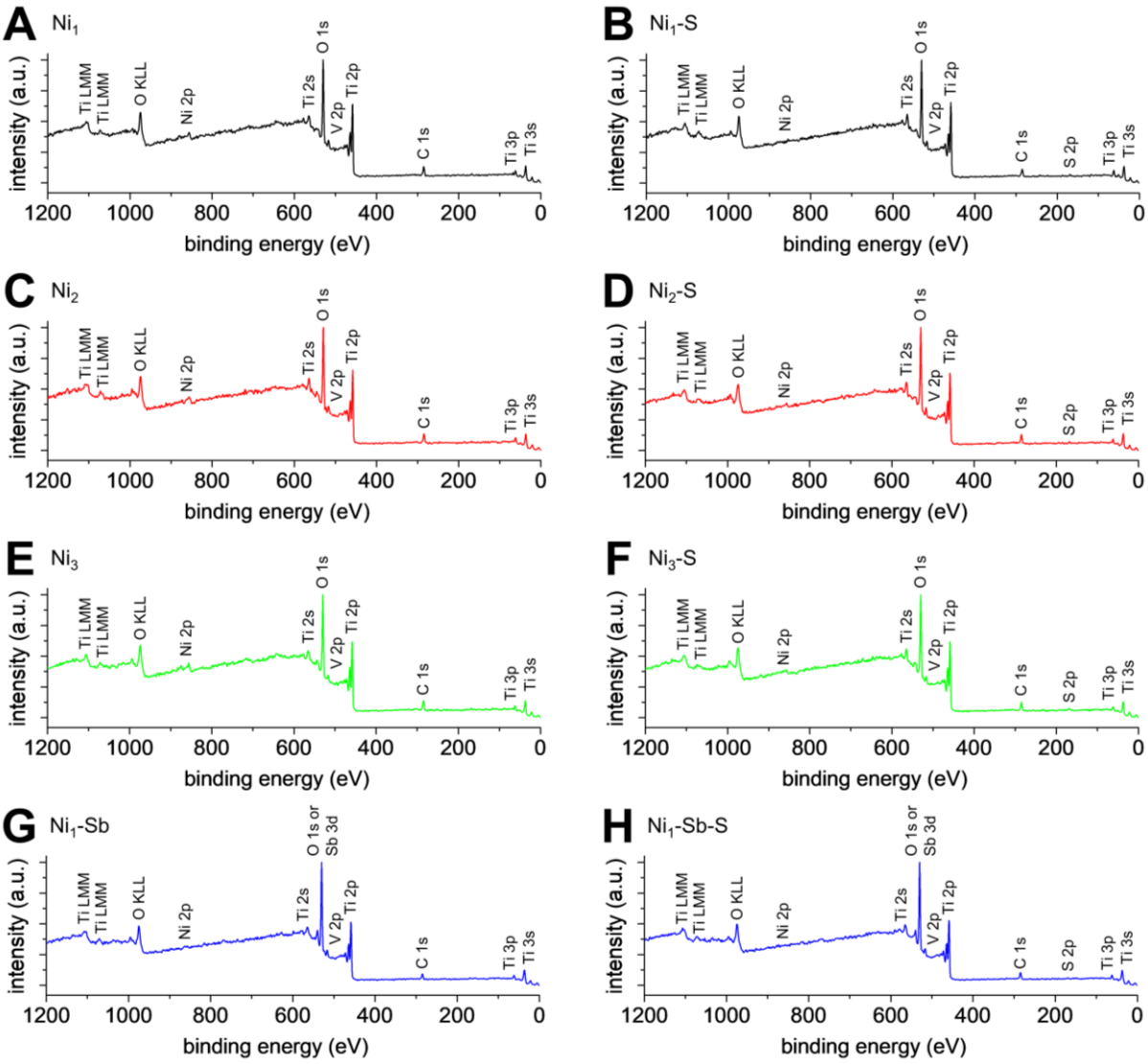

Fig. S2. Full scan survey of the XPS spectra for the catalysts (Ni_1 for A; Ni_2 for C; Ni_3 for E; Ni_1-Sb for G) and those functionalized with SO_Z^{2-}/HSO_Z^- (Ni_1-S for B; Ni_2-S for D; Ni_3-S for F; Ni_1-Sb-S for H). In (G-H), albeit with substantial overlaps between Sb 3d $_{5/2}$ and O 1s regimes at binding energies of 525.0-535.0 eV,[3, 4, 6] surface O compositions were in marked excess relative to their surface Sb counterparts. This thus made it highly sound that the XPS spectra of Ni_1-Sb and Ni_1-Sb-S at binding energies of 525.0-535.0 eV could be dictated by O of chemisorbed H_2O, labile O, and lattice O species.[4]

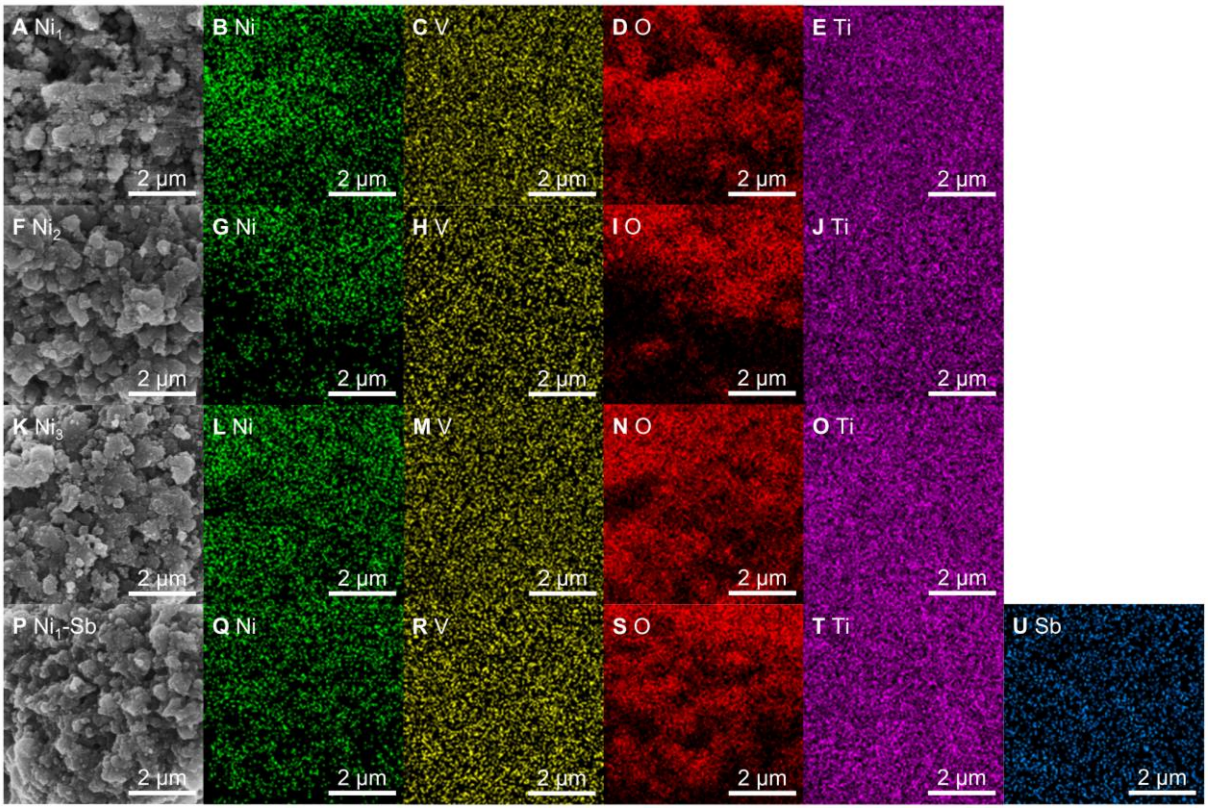

Fig. S3. EDX mapping images of the catalysts (Ni_1 for A-E; Ni_2 for F-J; Ni_3 for K-O; Ni_1-Sb for P-U).

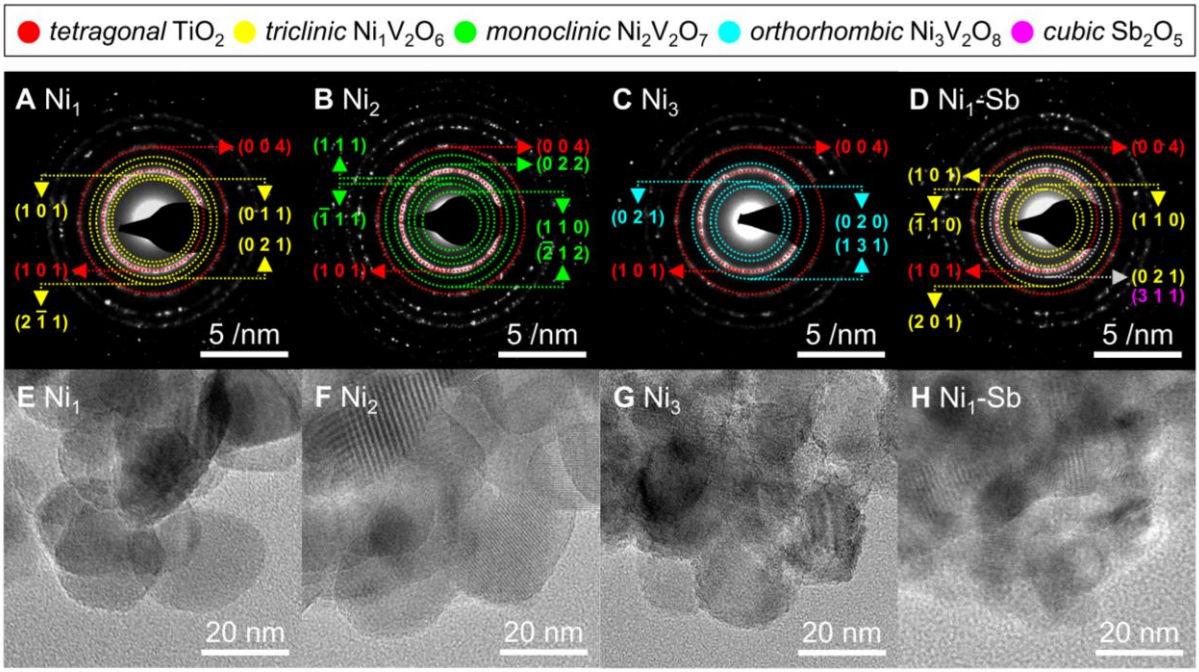

Fig. S4. SAED patterns (A-D) and HRTEM images (E-H) of the catalysts (Ni_1 for A and E; Ni_2 for B and F; Ni_3 for C and G; Ni_1-Sb for D and H). In (A-D), dashed circles indicate surface diffractions indexed to those of *tetragonal* TiO_2 (anatase, JCPDF No. of 01-071-1166), *triclinic* $Ni_1V_2O_6$ (JCPDF No. of 01-076-0359), *monoclinic* $Ni_2V_2O_7$ (JCPDF No. of 00-038-0285), *orthorhombic* $Ni_3V_2O_8$ (JCPDF No. of 01-070-2392), or *cubic* Sb_2O_5 (JCPDF No. of 00-011-0690). Surface diffractions with *d* spacing values of < 2.37 Å were not assigned due to significant overlaps among the diffractions of TiO_2, $Ni_1V_2O_6$, $Ni_2V_2O_7$, $Ni_3V_2O_8$, or Sb_2O_5.

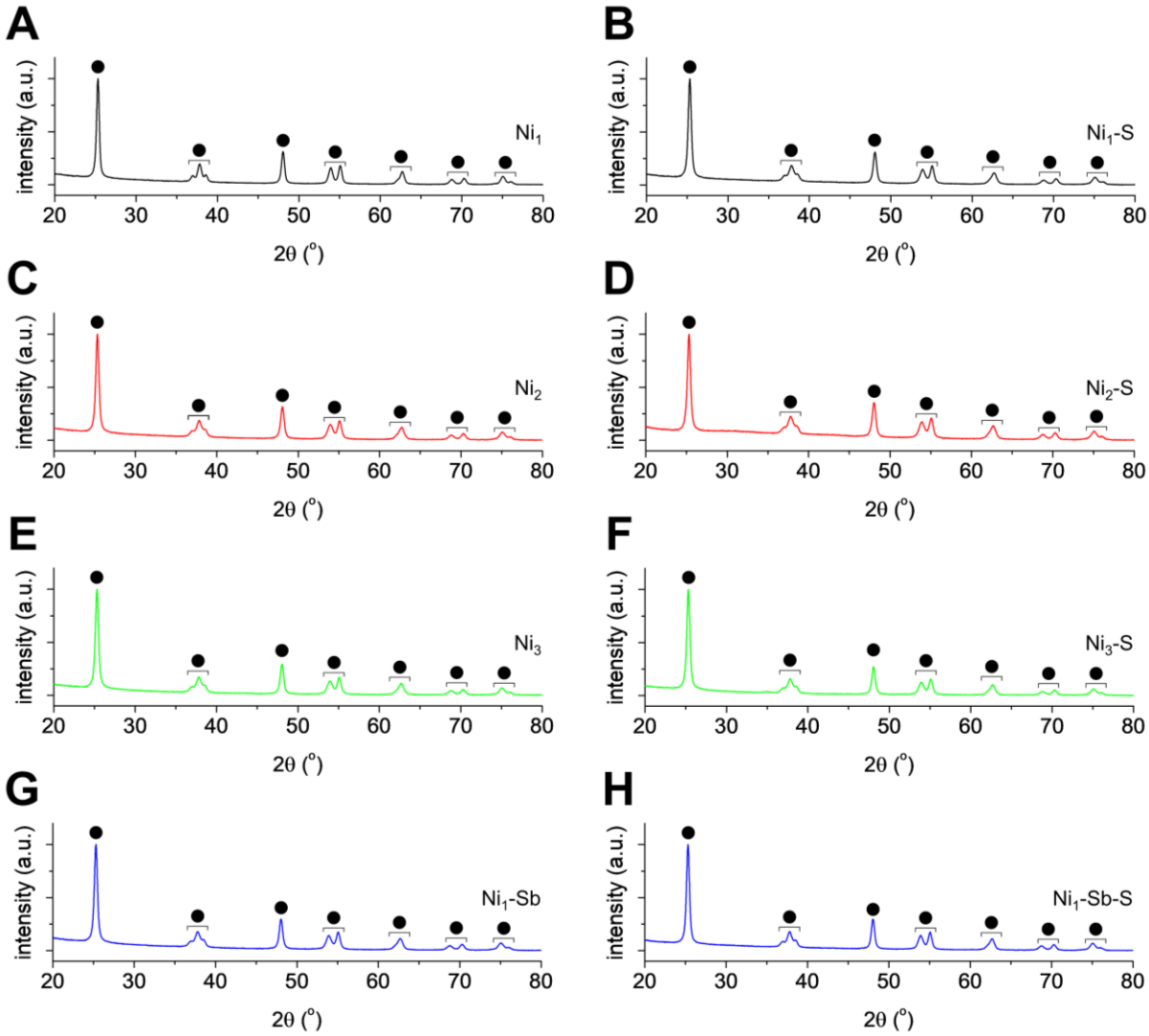

Fig. S5. XRD patterns of the catalysts (Ni_1 for A; Ni_2 for C; Ni_3 for E; Ni_1-Sb for G) and those functionalized with SO_z^{2-}/HSO_z^- (Ni_1-S for B; Ni_2-S for D; Ni_3-S for F; Ni_1-Sb-S for H). In (A-H), black solid circles denote bulk diffractions assigned to those of *tetragonal* TiO_2 (anatase, JCPDF No. of 01-071-1166).

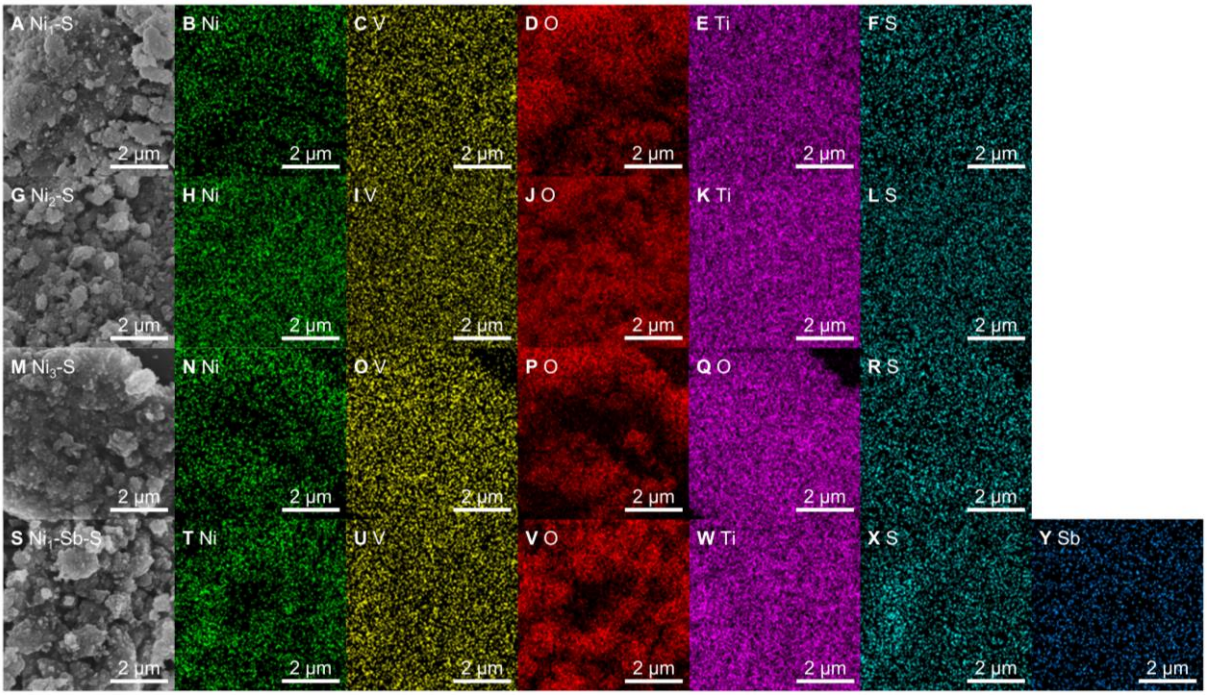

Fig. S6. EDX mapping images of the catalysts (Ni_1-S for A-F; Ni_2-S for G-L; Ni_3-S for M-R; Ni_1-Sb-S for S-Y).

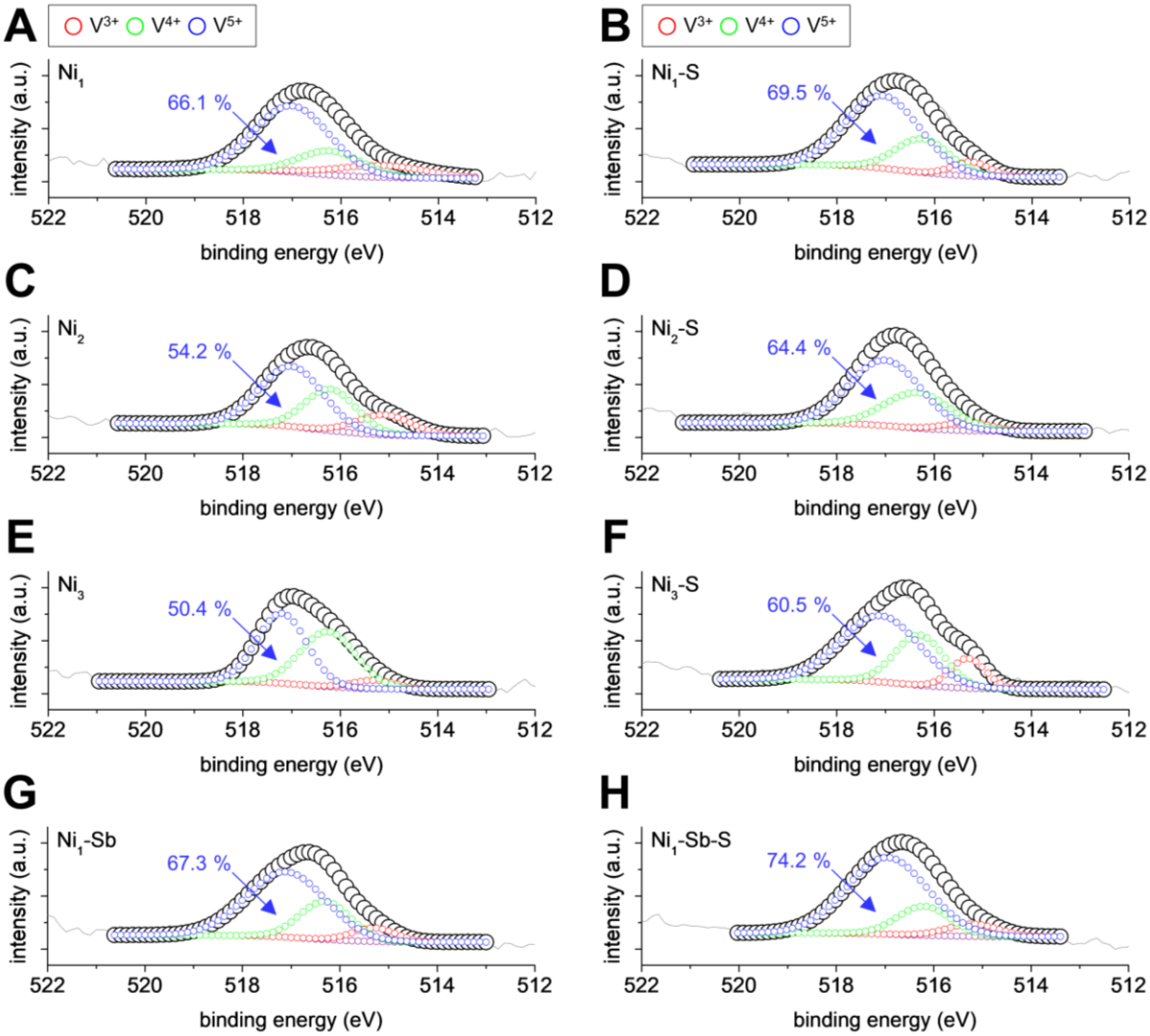

Fig. S7. XPS spectra of the catalysts (Ni_1 for A; Ni_2 for C; Ni_3 for E; Ni_1-Sb for G) and those functionalized with SO_z^{2-}/HSO_z^- (Ni_1-S for B; Ni_2-S for D; Ni_3-S for F; Ni_1-Sb-S for H) in the V 2p domains. In (A-H), gray solid lines and black empty circles denote raw and fitted spectra, respectively, whereas purple empty circles indicate backgrounds. In addition, red, green, and blue empty circles denote surface V^{3+}, V^{4+}, and V^{5+} phases, respectively.

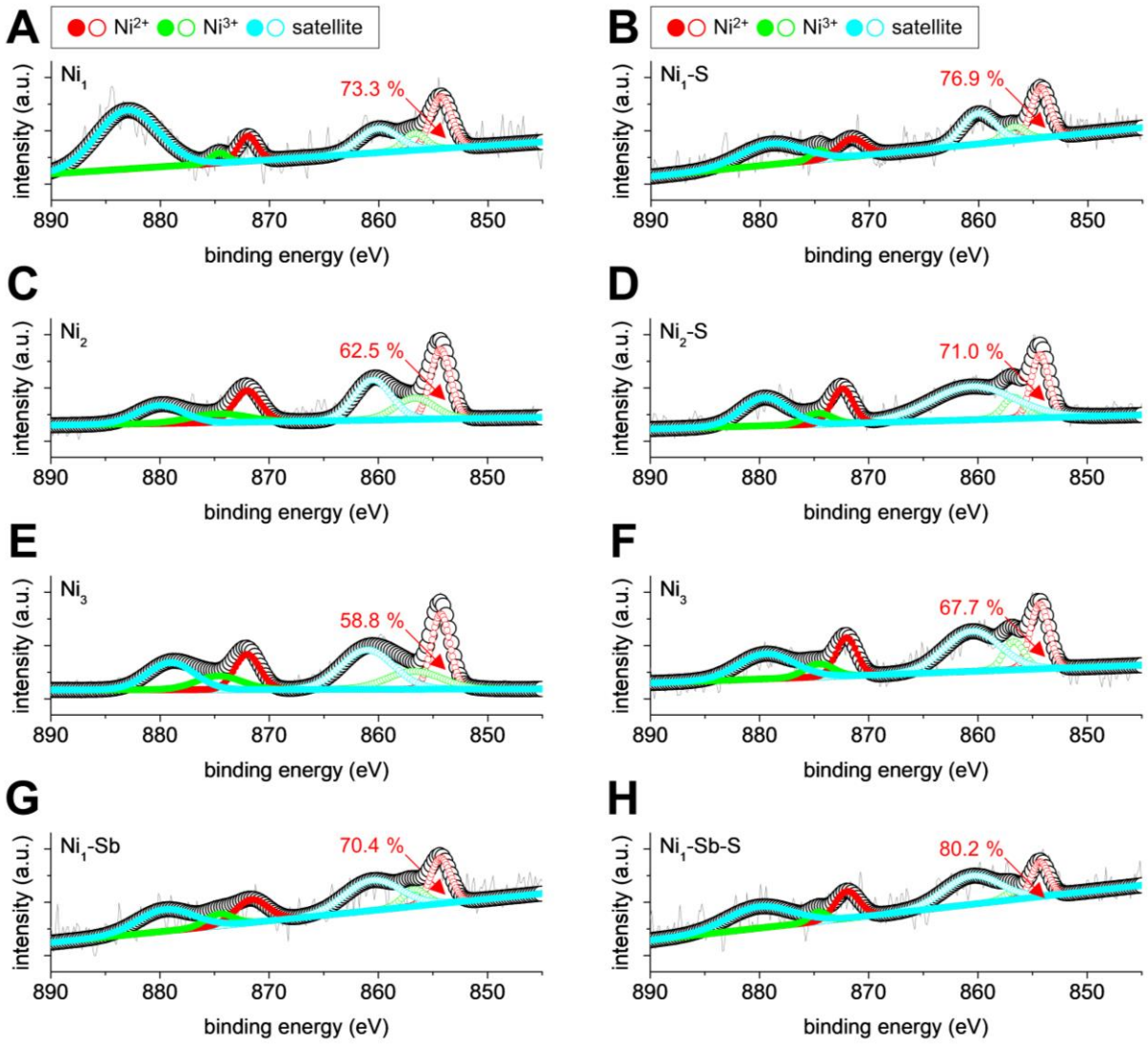

Fig. S8. XPS spectra of the catalysts (Ni_1 for A; Ni_2 for C; Ni_3 for E; Ni_1-Sb for G) and those functionalized with SO_Z^{2-}/HSO_Z^- (Ni_1-S for B; Ni_2-S for D; Ni_3-S for F; Ni_1-Sb-S for H) in the Ni 2p domains. In (A-H), gray solid lines and black empty circles denote raw and fitted spectra, respectively, whereas purple empty circles indicate backgrounds. In addition, red/green/cyan solid and empty circles denote surface Ni^{2+}/Ni^{3+}/satellite in the Ni 2p $_{1/2}$ and Ni 2p $_{3/2}$ regimes, respectively.

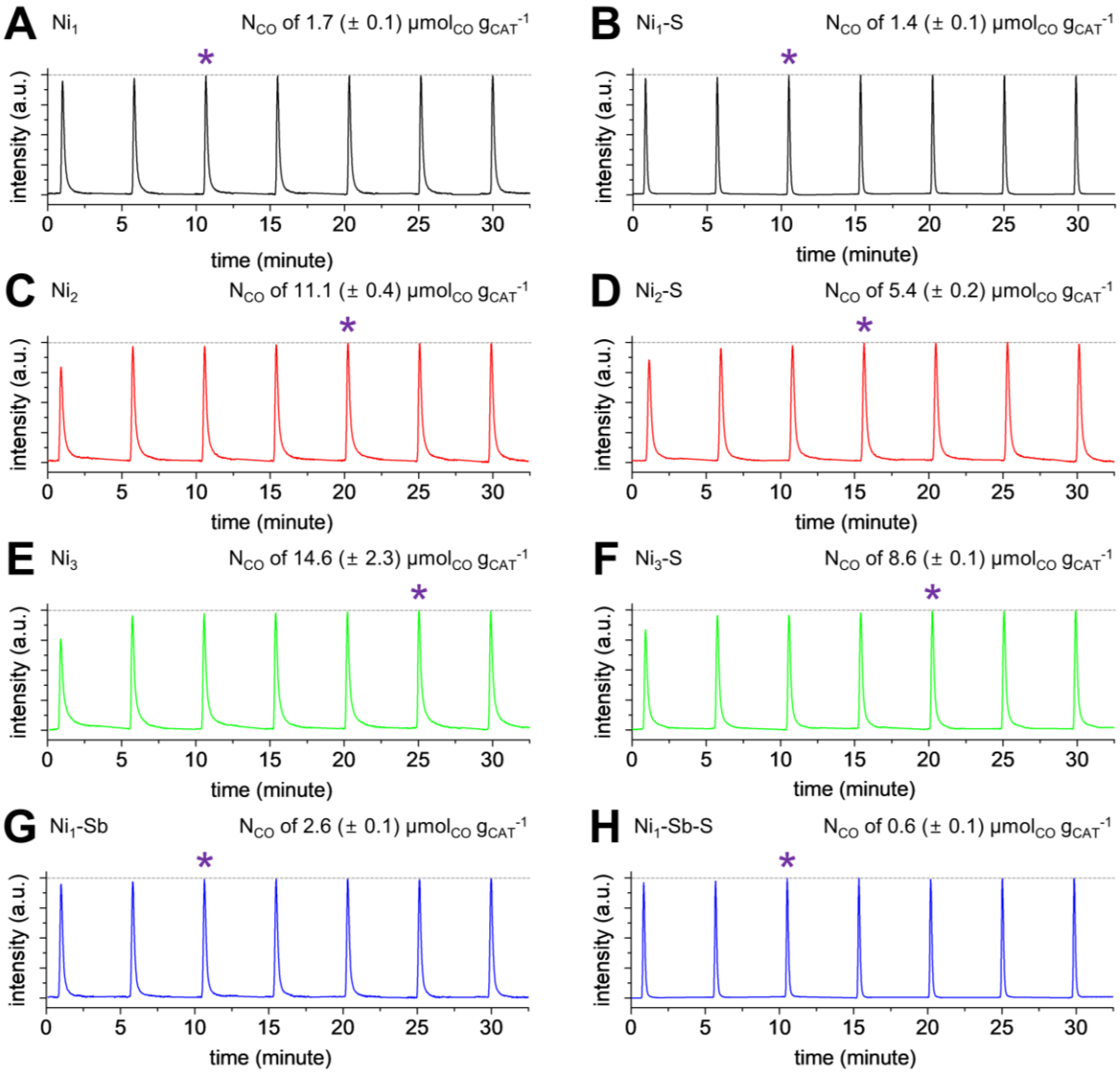

Fig. S9. CO-pulsed chemisorption profiles of the catalysts (Ni_1 for A; Ni_2 for C; Ni_3 for E; Ni_1-Sb for G) and those functionalized with SO_Z^{2-}/HSO_Z^- (Ni_1-S for B; Ni_2-S for D; Ni_3-S for F; Ni_1-Sb-S for H) at 50 °C. In (A-G), * corresponds to the onset of TCD signals for CO, whose intensities were almost invariant.

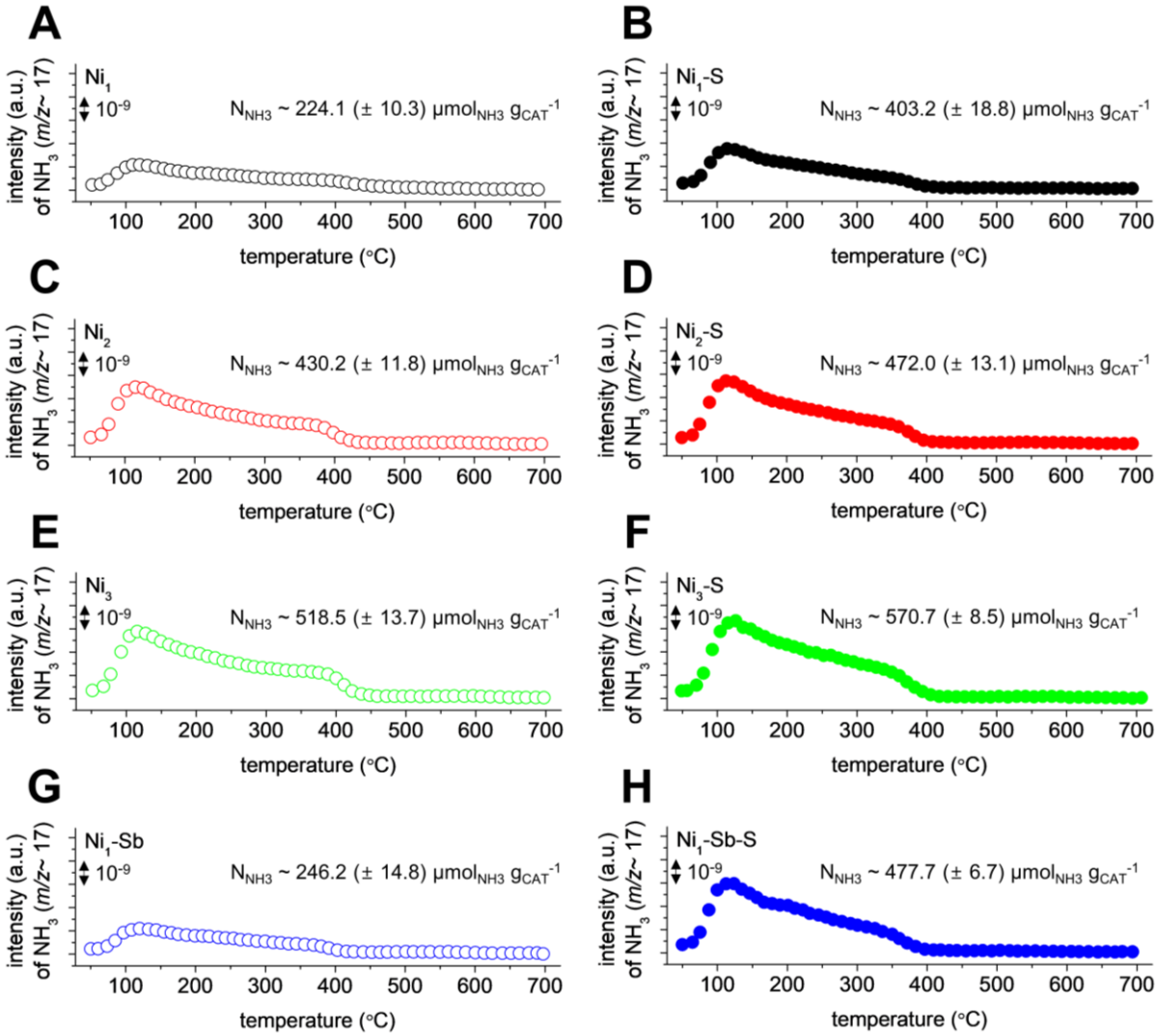

Fig. S10. NH_3-TPD profiles (NH_3 signal versus temperature) of the catalysts (Ni_1 for A; Ni_2 for C; Ni_3 for E; Ni_1-Sb for G) and those functionalized with SO_Z^{2-}/HSO_Z^- (Ni_1-S for B; Ni_2-S for D; Ni_3-S for F; Ni_1-Sb-S for H). The catalyst surfaces chemisorbed NH_3 at 50 °C and were then heated to 700 °C with a ramping rate of 10 °C min^{-1}. In (A-H), N_{NH3} values indicate the numbers of NH_3 adsorbed in a per-gram of the catalysts at 50 °C.

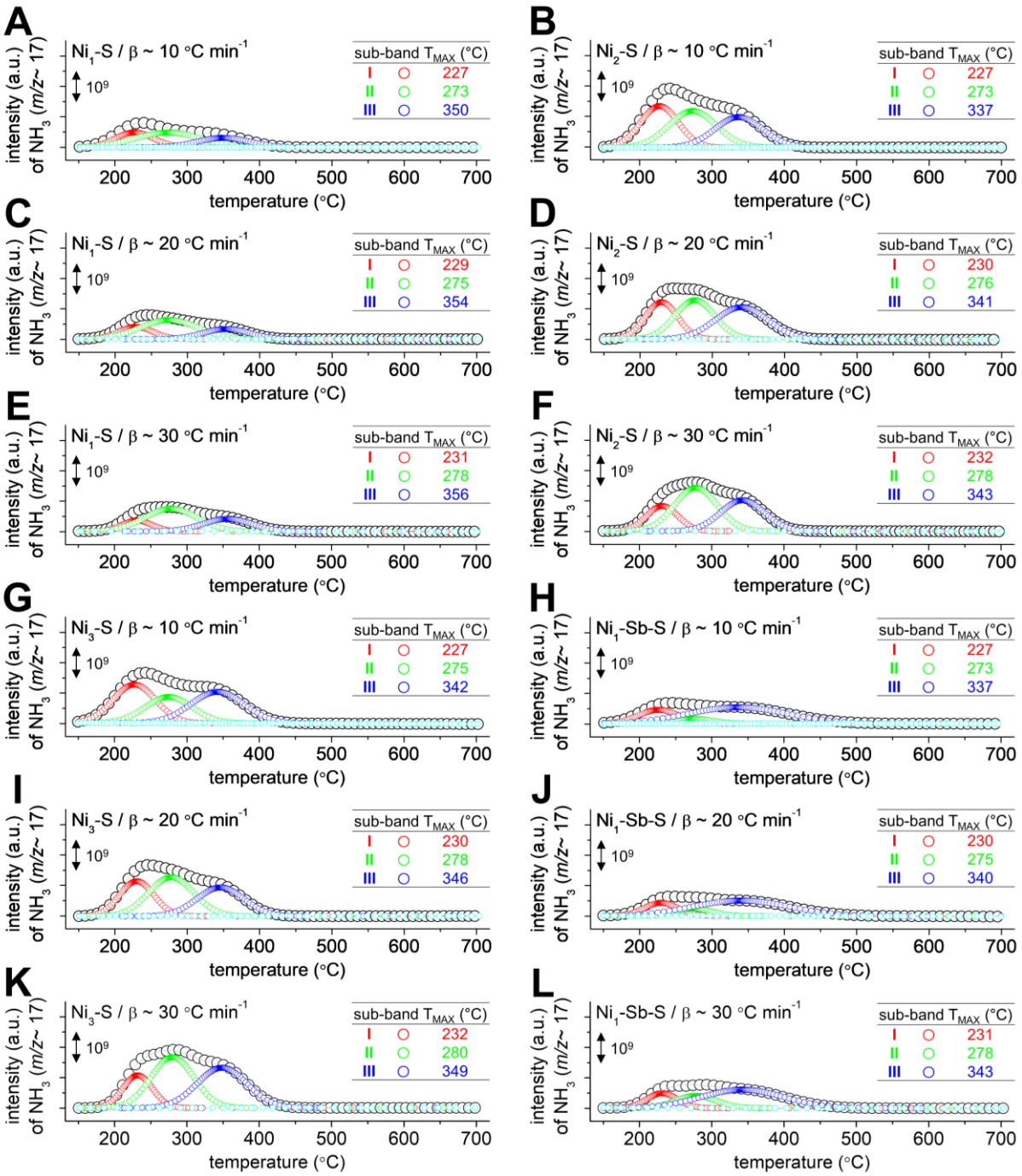

Fig. S11. NH_3-TPD profiles (NH_3 signal versus temperature) of the catalysts functionalized with SO_Z^{2-}/HSO_Z^- (Ni_1-S for A, C, and E; Ni_2-S for B, D, and F; Ni_3-S for G, I, and K; Ni_1-Sb-S for H, J, and L). The catalyst surfaces chemisorbed NH_3 at 150 °C and were then heated to 700 °C with a ramping rate (β) of 10 °C min^{-1} (A, B, G, and H), 20 °C min^{-1} (C, D, I, and J), or 30 °C min^{-1} (E, F, K, and L). In (A-L), NH_3-TPD profiles were de-convoluted using Gaussian function to reveal backgrounds (cyan empty circles) and three sub-bands (I (red empty circle), II (green empty circle), and III (blue empty circle)), whose temperatures with maximum NH_3 signal intensities (T_{MAX}) are presented in inset tables and served to assess NH_3 binding energies (E_{NH3}) of the catalyst surfaces at 150 °C.

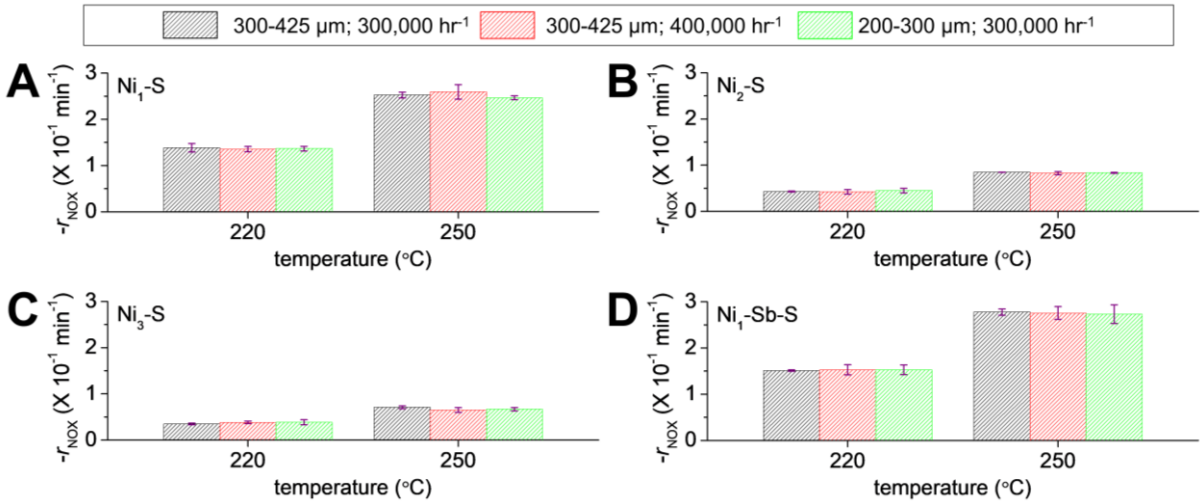

Fig. S12. NO_X consumption rates ($-r_{NOX}$) of the catalysts upon the change in their particle sizes (200-300 μm or 300-425 μm) or space velocities (300,000 hr^{-1} or 400,000 hr^{-1}) at 220 and 250 °C (Ni_1-S for A; Ni_2-S for B; Ni_3-S for C; Ni_1-Sb-S for D). SCR conditions: 800 ppm NO_X; 800 ppm NH_3; 3 vol. % O_2; 5.4 vol. % H_2O; total flow rate of 500 mL min^{-1}; balanced by a N_2.

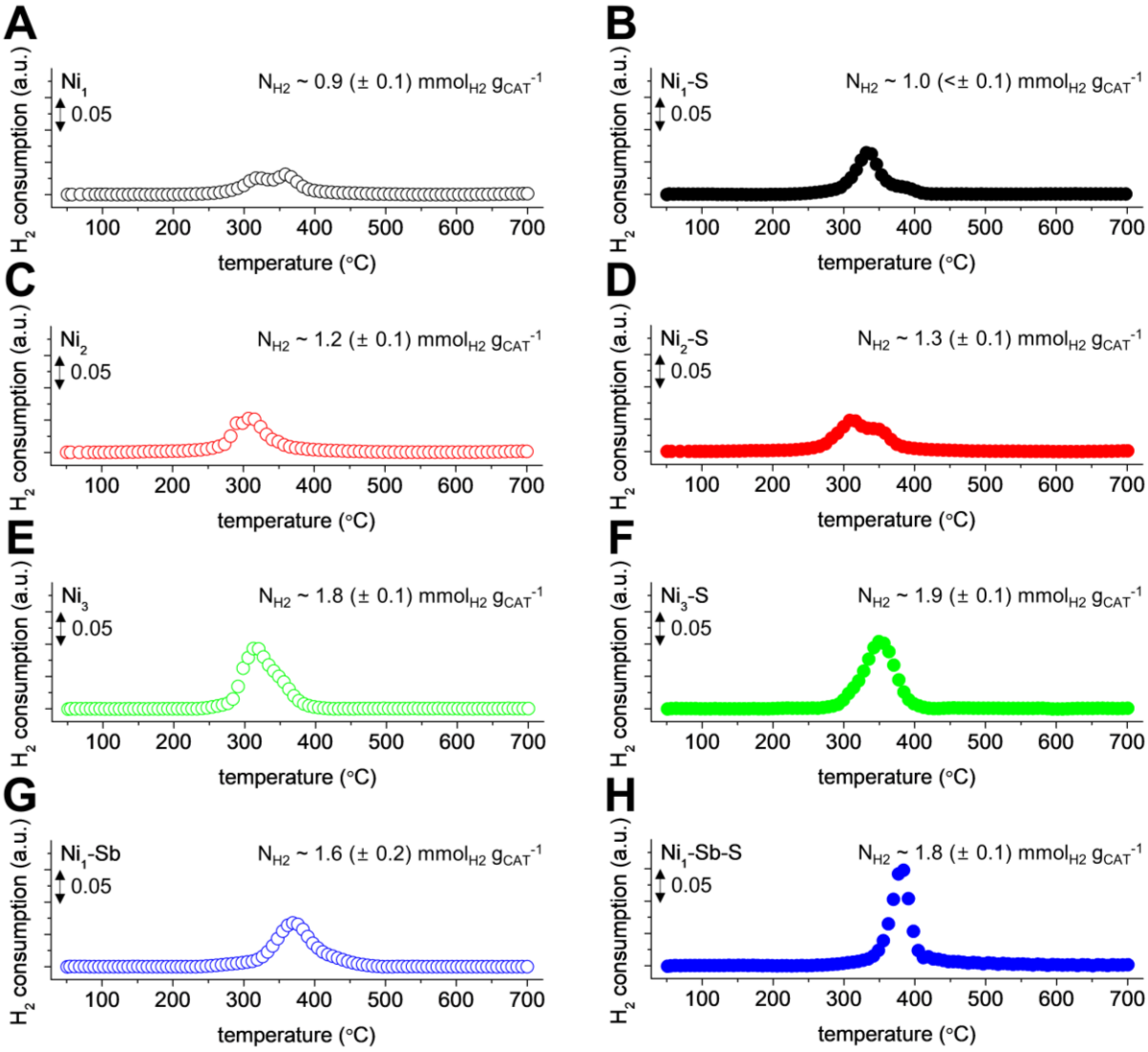

Fig. S13. H_2-TPR profiles (TCD signal versus temperature) of the catalysts (Ni_1 for A; Ni_2 for C; Ni_3 for E; Ni_1-Sb for G) and those functionalized with SO_Z^{2-}/HSO_Z^- (Ni_1-S for B; Ni_2-S for D; Ni_3-S for F; Ni_1-Sb-S for H). The catalyst surfaces were reduced with H_2 at 50-700 °C with a ramping rate of 10 °C min^{-1}. In (A-H), N_{H2} values indicate the numbers of H_2 needed to reduce a gram of the catalysts.

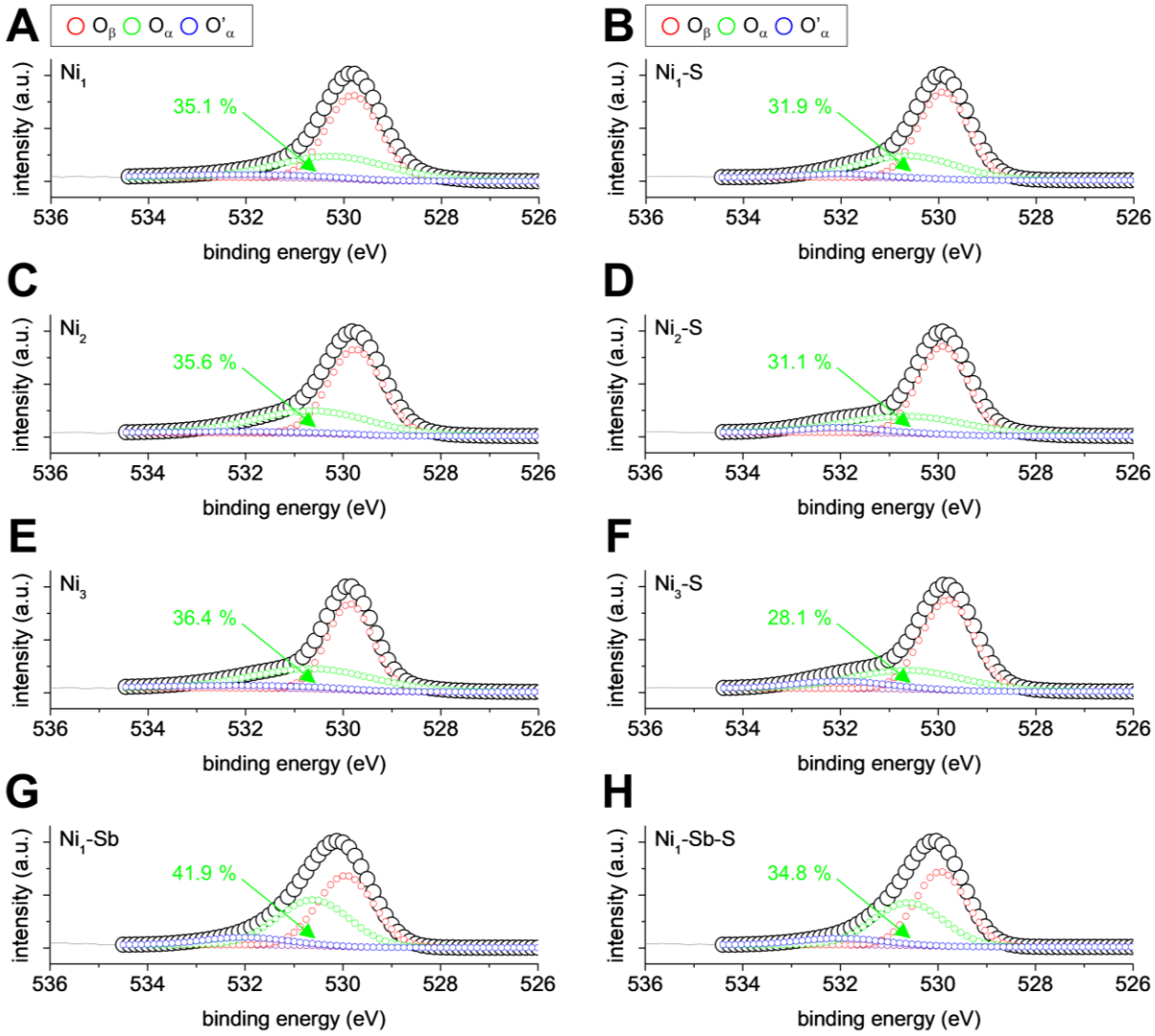

Fig. S14. XPS spectra of the catalysts (Ni_1 for A; Ni_2 for C; Ni_3 for E; Ni_1-Sb for G) and those functionalized with SO_Z^{2-}/HSO_Z^- (Ni_1-S for B; Ni_2-S for D; Ni_3-S for F; Ni_1-Sb for H) in the O 1s domains. In (A-F), gray solid lines and black empty circles denote raw and fitted spectra, respectively, whereas purple empty circles indicate backgrounds. In addition, red, green, and blue empty circles denote surface O_β, O_α, and O'_α phases, respectively.

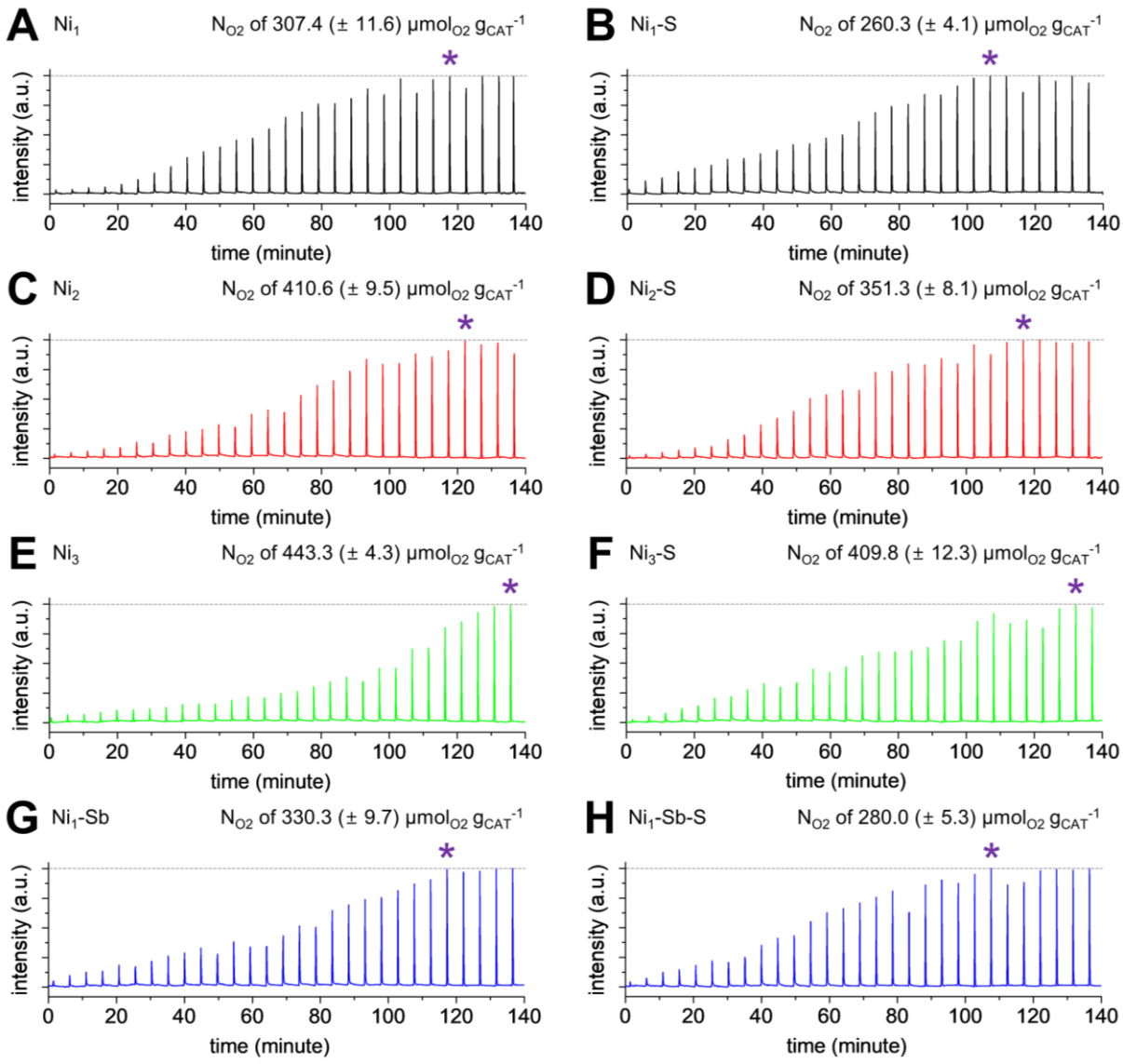

Fig. S15. O_2-pulsed chemisorption profiles of the catalysts (Ni_1 for A; Ni_2 for C; Ni_3 for E; Ni_1-Sb for G) and those functionalized with SO_Z^{2-}/HSO_Z^- (Ni_1-S for B; Ni_2-S for D; Ni_3-S for F; Ni_1-Sb-S for H) at 250 °C. In (A-G), * corresponds to the onset of TCD signals for O_2, whose intensities were almost invariant.

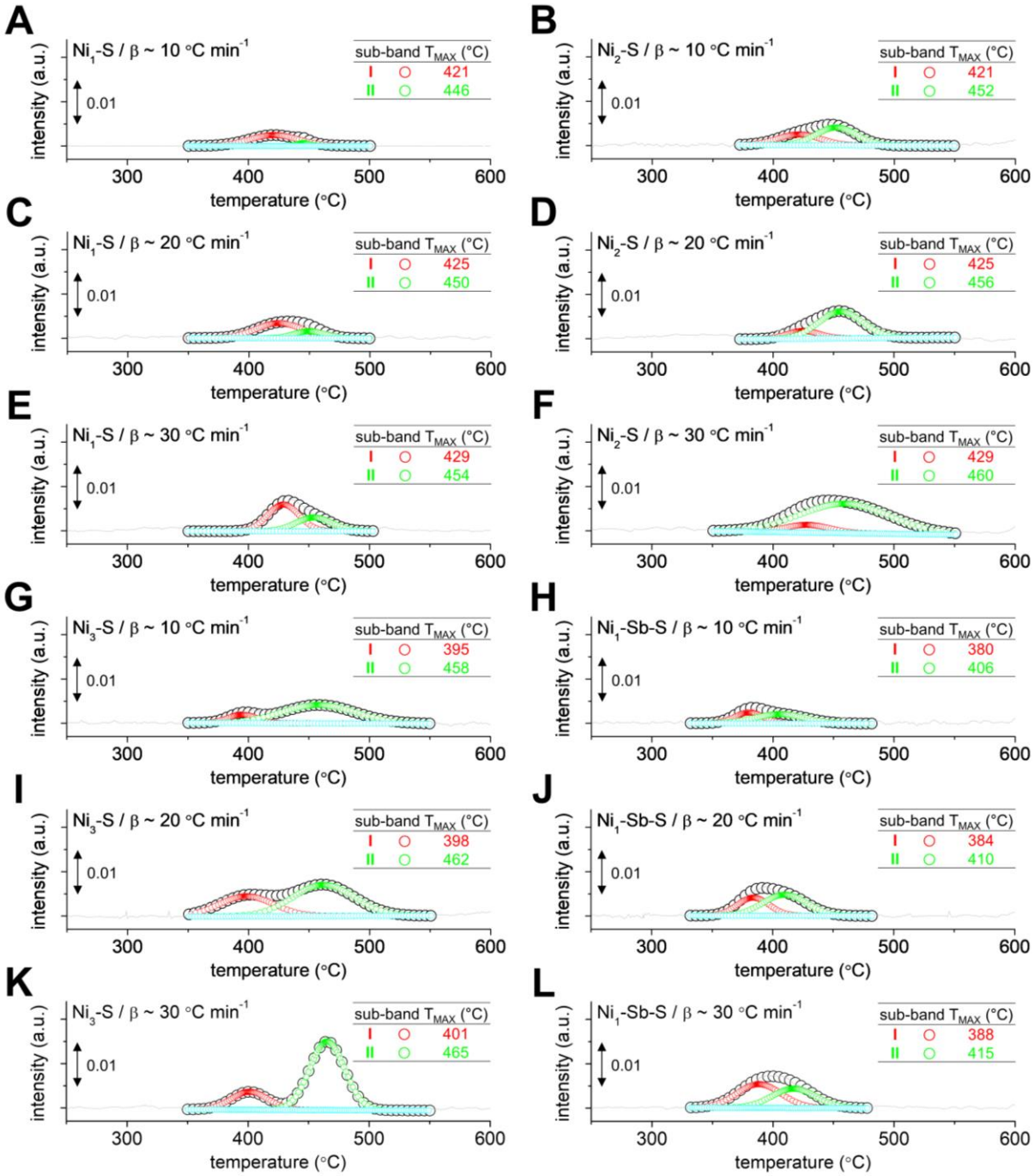

Fig. S16. O_2-TPD profiles (TCD signal versus temperature) of the catalysts functionalized with SO_Z^{2-}/HSO_Z^- (Ni_1-S for A, C, and E; Ni_2-S for B, D, and F; Ni_3-S for G, I, and K; Ni_1-Sb-S for H, J, and L). The catalyst surfaces were reduced with H_2 at 300 °C for an hour, cooled to 250 °C, chemisorbed O_2 at 250 °C, and were then heated to 600 °C with a ramping rate (β) of 10 °C min^{-1} (A, B, G, and H), 20 °C min^{-1} (C, D, I, and J), or 30 °C min^{-1} (E, F, K, and L). In (A-L), O_2-TPD profiles were de-convoluted using Gaussian function to reveal backgrounds (cyan empty circles) and two sub-bands (I (red empty circle) and II (green empty circle)), whose temperatures with maximum TCD signal intensities (T_{MAX}) are presented in inset tables and served to assess O_2 binding energies ($E_{OL/OM}$) of the catalyst surfaces at 250 °C.

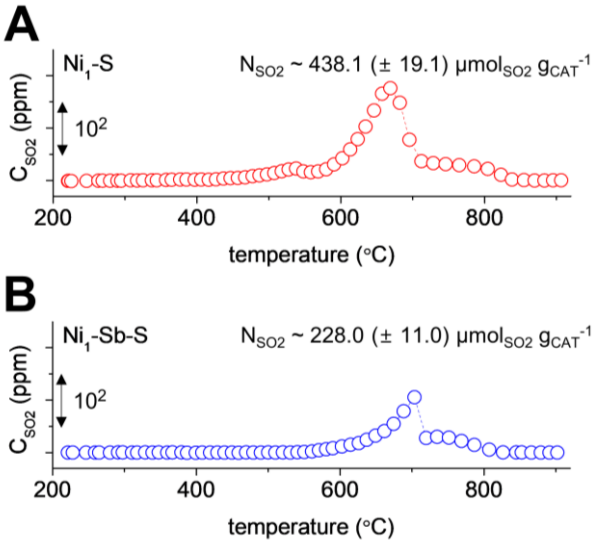

Fig. S17. SO_2-TPD profiles (SO_2 concentration (C_{SO2}) versus temperature) of the catalysts functionalized with SO_Z^{2-}/HSO_Z^- (Ni_1-S for A; Ni_1-Sb-S for B). The catalyst surfaces chemisorbed SO_2 at 220 °C and were then heated to 900 °C with a ramping rate of 10 °C min^{-1}. In (A-C), N_{SO2} values indicate the numbers of SO_2 adsorbed in a per-gram of the catalysts at 220 °C.

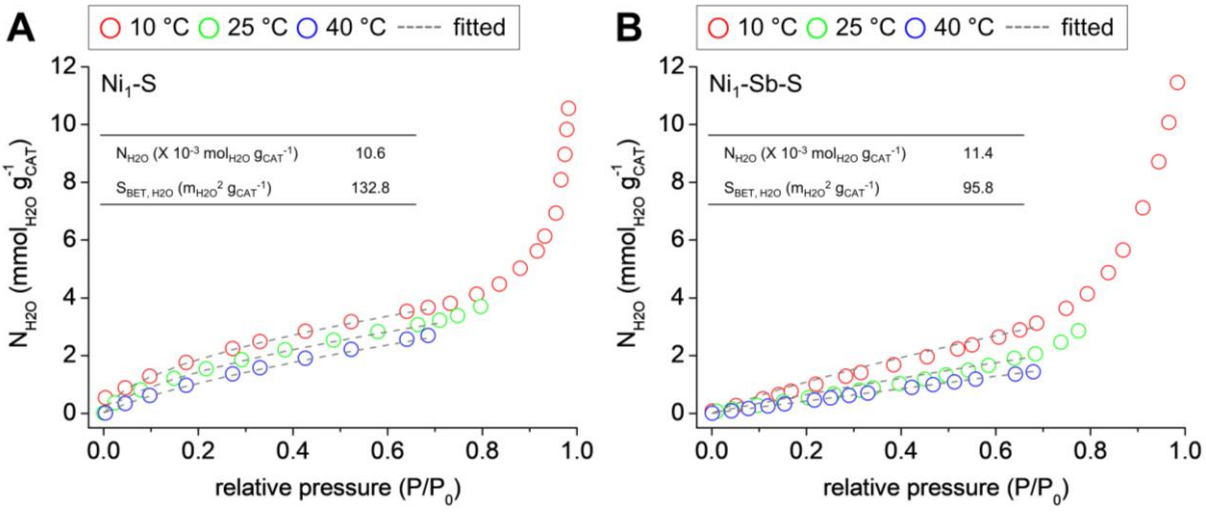

Fig. S18. H_2O adsorption isotherms of Ni_1-S (A) and Ni_1-Sb-S (B). In (A-B), red, green, and blue empty circles denote H_2O adsorption isotherms collected at 10 °C, 25 °C, and 40 °C, respectively, whereas gray dashed lines denote H_2O adsorption isotherms simulated using Toth equation. In addition, inset tables contain the numbers of H_2O adsorbed in a per-gram of the catalysts (N_{H2O}) at partial pressure (P/P_0) of ~1.0 and 10 °C alongside with H_2O-accessible BET surface areas in a per-gram of the catalysts ($S_{BET, H2O}$) at 10 °C.

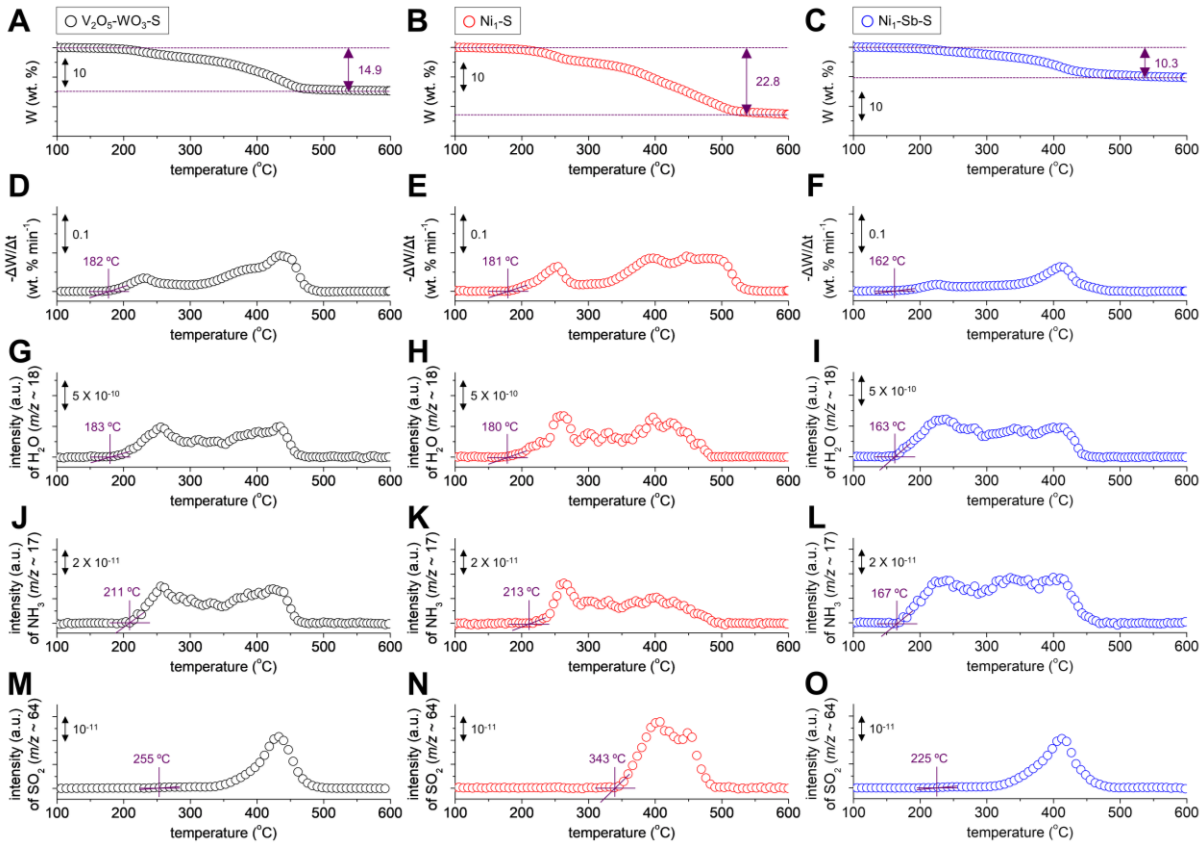

Fig. S19. Profiles of weight percent loss versus temperature (V_2O_5-WO_3-S for A; Ni_1-S for B; Ni_1-Sb-S for C), the 1st derivative of weight percent loss with respect to time versus temperature (V_2O_5-WO_3-S for D; Ni_1-S for E; Ni_1-Sb-S for F), and signals of H_2O (V_2O_5-WO_3-S for G; Ni_1-S for H; Ni_1-Sb-S for I), NH_3 (V_2O_5-WO_3-S for J; Ni_1-S for K; Ni_1-Sb-S for L), and SO_2 (V_2O_5-WO_3-S for M; Ni_1-S for N; Ni_1-Sb-S for O) released versus temperature for the catalysts poisoned with AS/ABS under an Ar. In (A-C), values shown with arrows denote the quantities of AS/ABS (wt. %) included in the poisoned catalysts. In (D-O), temperatures denoted the onsets, where the weight loss or H_2O/NH_3/SO_2 signal evolution was initiated. AS/ABS degradation conditions: flow rate of 50 mL min^{-1}; ramping rate of 2 °C min^{-1}.

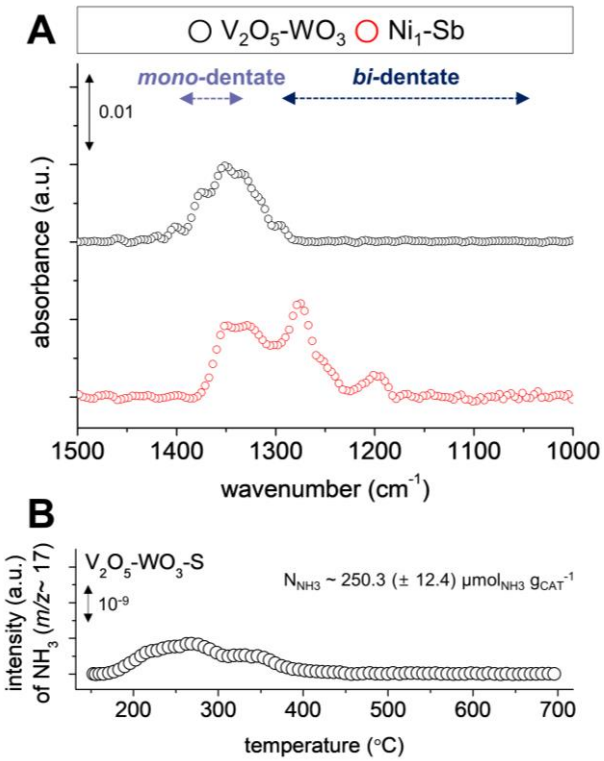

Fig. S20. (A) Background-subtracted *in situ* SO_2/O_2-DRIFT spectra of V_2O_5-WO_3 and Ni_1-Sb exposed to $SO_2/O_2/N_2$ at 500 °C with a ramping rate of 10 °C min^{-1} and a total flow rate of 200 mL min^{-1}. Background-subtracted *in situ* SO_2/O_2-DRIFT spectrum of Ni_1-Sb is re-plotted for comparison. (B) NH_3-TPD profile (NH_3 signal versus temperature) of V_2O_5-WO_3-S. V_2O_5-WO_3-S surface chemisorbed NH_3 at 150 °C and was then heated to 700 °C with a ramping rate of 10 °C min^{-1}. In (B), N_{NH3} indicates the number of NH_3 adsorbed in a per-gram of V_2O_5-WO_3-S at 150 °C.

References

1. J. Kim, D. W. Kwon, S. Lee and H. P. Ha, *Appl. Catal. B*, 2018, **236**, 314-325.
2. J. Kim, D. H. Kim and H. P. Ha, *J. Hazard. Mater.*, 2020, **397**, 122671.
3. S. Lee, J.-H. Lee, H. P. Ha and J. Kim, *Chem. Mater.*, 2022, **34**, 1078-1097.
4. J. Kim, D. H. Kim, J. Park, K. Jeong and H. P. Ha, *ACS Catal.*, 2022, **12**, 2086-2107.
5. H. J. An, D. H. Kim, H. P. Ha and J. Kim, *J. Mater. Chem. A*, 2021, **9**, 8350-8371.
6. J. Kim, K. B. Nam and H. P. Ha, *J. Hazard. Mater.*, 2021, **416**, 125780.
7. Y. Yang, Z. Qiu, G. Weng, H. Wang, Y. Li, B. Fan, X. Bai, Q. Zhang and C. Chen, *Adv. Funct. Mater.*, 2022, **32**, 2106828.
8. H. Ahn and C.-H. Lee, *Chem. Eng. Sci.*, 2004, **59**, 2727-2743.
9. D. Chen, X. Hu, L. Shi, Q. Cui, H. Wang and H. Yao, *Appl. Clay Sci.*, 2012, **59-60**, 148-151.
10. D. H. Kim, S.-H. Oh, H. P. Ha, Y.-C. Joo and J. Kim, *Appl. Surf. Sci.*, 2023, **614**, 156099.
11. M. Kim, J. Park, S. H. Kim, J.-H. Lee, K. Jeong and J. Kim, *Carbon*, 2023, **203**, 630-649.
12. Y. J. Choe, S. H. Kim, K. Jeong and J. Kim, *Chem. Eng. J.*, 2023, **455**, 140537.
13. Y. J. Choe, S. Lee, M. Kim, S. H. Kim, I.-S. Choi, K. Jeong and J. Kim, *Sep. Purif. Technol.*, 2023, **310**, 123146.
14. J. Kim, Y. J. Choe and S. H. Kim, *Chem. Eng. J.*, 2021, **413**, 127550.
15. J. Kim, Y. J. Choe, S. H. Kim, I.-S. Choi and K. Jeong, *JACS Au*, 2021, **1**, 1158-1177.
16. Y. J. Choe, S. H. Kim, K. Jeong and J. Kim, *Chem. Eng. J.*, 2022, **455**, 140537.
17. J. Kim, S. Lee and H. P. Ha, *ACS Catal.*, 2021, **11**, 767-786.